

國立臺灣大學理學院化學系

碩士論文

Department of Chemistry

College of Science

National Taiwan University

Master Thesis



3號位取代硫二苯胺的初步光物理特性

Rudimentary photophysical property of selected 3-substituted
phenothiazines

陳孟圻

Meng-Chi Chen

指導教授：周必泰 博士

Advisor: Pi-Tai Chou, Ph.D.

中華民國 109 年 1 月

January 2020

國立臺灣大學碩士學位論文
口試委員會審定書

論文中文題目 3 號位取代硫二苯胺的初步光物理特性

論文英文題目 Rudimentary photophysical property of selected
3-substituted phenothiazines

本論文係 陳孟圻 君 (學號 R06223192) 在國立臺灣大學化學系完成之碩士學位論文，於民國 109 年 1 月 16 日承下列考試委員審查通過及口試及格，特此證明。

口試委員：

周心昇 (簽名)
(指導教授)

張鈺平

張鈺平

系主任、所長 梁文傑 (簽章)

致謝



自 2016 年六月從國立清華大學化學系畢業後，經歷了一年半的顛簸，我在 2018 年二月才重新回到校園。在這一年半中，十月服完兵役、十一月申請國外研究所失利、十二月匆忙準備考國內研究所；隔年初發現國內國外研究所皆落榜，於是決定念完碩士再出國。開始蹲研究所補習班，虛心地將自己學識不足的地方補齊。整個 2017 年，我將大學化學完整地複習了一遍。十月申請臺大化學碩士班甄試，在經過書面審查及口試後，儘管落在備取的安全名單內，但仍孜孜不倦地準備並報名隔年初的碩士班考試。在 2018 年的一月，我先是得知甄試備取錄取通知，隨後參加研究所考試，接著用甄試錄取的管道申請提早入學，並於二月初正式加入周必泰實驗室，最後於二月中得知碩士班考試獲得正取 13 的成績。

藉由甄試與考試兩個不同性質的管道，我都能錄取臺大化學系。這並不是因為我優秀，而是一路上有許多人的協助。其中，在準備甄試與考試的過程中，有一群在補習班認識的戰友彼此切磋砥礪。臺大植微趙子瑄；師大化學蘇尹翔、吳世鴻、吳承軒、徐儷文、陳彥瑜、黃柏元；淡江化學陳昱涵、呂曉旻、方博靖、賴雨岑；臺大化學顏竹君、張達生，交大化學許亮宇、輔大化學廖又潔、中原化學高琛華、北市教大呂佳澄。以上同學讓我在準備考試的路上不孤單。另外，在給臺大化學的推薦信中，多虧了在清華大學時的專題指導老師黃哲勳教授，以及大學期間去美國 UC San Diego 交換研究生時指導我的博後 Dr. Juan Luis Bosch 的大力支持，我才能夠申請順利。

進入周必泰實驗室的第一年，我在奈米組做量子點的研究。第二年轉入光譜組，進行本論文的研究。奈米組的周尚威博士、胡育愷、陳晏誼、周克駿、李衍毅、黃智炫、劉怡均，及羅子軒，都給我許多支持。光譜組的劉士弘博士、陳怡安博士、陳怡廷博士、陳登高、劉宗穎、魏佑臣、張凱信、鄭郁璇、曾聖茗、黃俊穎、林家安、王致惟、周大喆、林千妍、陳奕云、盧宥霖、Seb Jackson，及吳秀剛，在實驗上給我許多協助。我想特別提一下陳登高學長，他給我許多研究上的幫助，在我看來，他不只是

位博士生，而是位已經有助理教授學識與氣度的科學家。有機組的陳怡博士、孟繁翌博士、劉俊騏、李曜麟、何愷愉、楊雨軒、彭宇強，及何嘉哲，也讓我成長不少。

周必泰老師是位刀子嘴豆腐心的好老師。表現不佳時他罵得很難聽，是希望我們可以進步。老師百忙之中還願意幫我寫國外研究所跟獎學金的推薦信，我十分感動。實驗室助理林佳貞幫助大家處理報帳等行政工作，讓大家可以專心於研究。系辦許慧禎小姐從我提早入學時的申請，到我畢業時的口試與離校都給予許多協助。

先父陳守文在我畢業半年前因腎臟病末期辭世，我很開心他可以看見我大學畢業，可惜無法看見我碩士畢業。處理父親後事的過程，身為獨生子的我責無旁貸。喪假期間周老師及實驗室同仁的包容我沒齒難忘，請假去參與後續法事老師也十分寬容。當我在龍巖為父親守靈時，李曜麟同學還不忘以電郵及電話不斷地督促我整理數據並盡快撰寫期刊草稿，真是令人動容。

家人方面，阿嬤陳蔡阿嬌、先父陳守文，及母親張麗玲提供了一個可以自由追夢的家，讓我專心於學業、研究，及申請國外大學。雙親生給我健全的身體，讓我可以忍受追求知識的過程中必要之身心靈的壓力。每天開車上下班的呂佳燕對我這個每天騎腳踏車上下學的男友不離不棄，如此寬大的胸襟實在是有容乃大。這一路走來我接受的幫助實在是太多了，孟圻在此向各位深深一鞠躬。

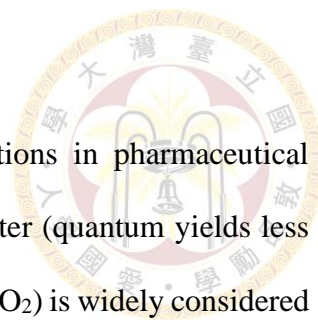
摘要



無論在藥物、染料敏化太陽能電池，或是有機發光二極體上，硫二苯胺（phenothiazine，**PTZ**）都有許多的應用。但由於它螢光量子產率低（在環己烷中小於1%），在應用上受到部分限制。有趣的是，當這個低螢光量子產率與硝基（-NO₂），一個普遍公認螢光淬滅體，結合形成 3-硝基硫二苯胺（3-nitrophenothiazine，**PTZ-NO₂**）時，竟有極高的螢光量子產率（在環己烷中100%）。為了更進一步調查此現象及其背後的物理化學機制，我們設計並合成了一系列的 C3 取代硫二苯胺來做比較，其中取代基包含拉電子的腈基（-CN）、甲醯基（-CHO），及硝基（-NO₂），以及推電子的甲氧基（-OMe）。與無取代的硫二苯胺及加了推電子基的硫二苯胺相比，拉電子基造成螢光量子產率明顯提高。在化學計算的幫助之下，我們發現 π 到 π^* 的電子躍遷在 **PTZ** 及 **PTZ-OMe** 中是部分禁制躍遷，因其 π^* 與硫上的未鍵結軌域混合；相反地，由於拉電子基降低了 LUMO 的能量，使它不再與未鍵結軌域混合，而造成 π 到 π^* 變為容許躍遷。此研究展示了如何利用分子設計一窺 **PTZ** 中 HOMO 跟 LUMO 的能量，進而達到高螢光量子產率。

關鍵字：硫二苯胺、硝基、量子產率、螢光。

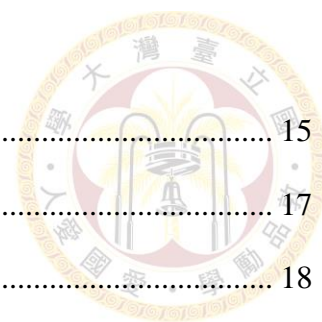
Abstract



Phenothiazine (**PTZ**) is a versatile compound that possesses many applications in pharmaceutical chemistry, dye-sensitized solar cell, etc. However, its weak-fluorescent character (quantum yields less than 1% in toluene) impedes its further applications. Besides, the nitro group (-NO₂) is widely considered as a fluorescence quencher. Interestingly, we can obtain a highly fluorescent chromophore by combining these two moieties, forming 3-nitrophenothiazine (**PTZ-NO₂**). To make a fair comparison, a series of **PTZ** substituted with various electron-withdrawing groups (cyano **-CN** and formyl **-CHO**) and electron-donating group (methoxy **-OMe**) group at C3-position was designed and synthesized. As we observed, the three molecules with different electron-withdrawing groups exhibit brilliant quantum yields compared with the non-substituted **PTZ** and electron-donating group substituted derivative. With the aid of computational approaches, the results reveal that the electronic transitions in **PTZ** and **PTZ-OMe** are partially forbidden π to π^* transition, in which the π^* orbital is mixed with the nonbonding orbital character of the sulfur atom. On the contrary, the transitions in the electron-withdrawing substituted analogies show allowed π to π^* transition, which is due to the addition of electron-withdrawing group lowering the energy level of LUMO to diminish their mixing with non-bonding orbitals. This work demonstrates a judicious chemical design to exploit the energy level of HOMO and LUMO in **PTZ** analogies to achieve the high quantum yields.

Keywords: phenothiazine, nitro, quantum yield, fluorescence.

Contents



I. Introduction.....	15
II. Motivation.....	17
III. Experiments	18
A. Synthesis	18
B. Absorbance.....	19
C. Photoluminescence.....	19
D. Quantum yield.....	20
E. Time-Correlated Single Photon Counting (TCSPC).....	21
F. Extinction coefficient.....	21
G. Thermal vapor deposition	22
IV. Results and Discussion	24
A. Structural Characterization	24
V. Solid state photophysical property of PTZ-NO ₂	24
A. Photophysical properties	25
B. Cyclic voltammetry analysis.....	28
C. Computational approaches.....	30
VI. Conclusion	33
VII. Spectra, computed frontier orbitals, and additional tables	34
A. Absorption and Fluorescence in cyclohexane, toluene and dichloromethane	34
B. Absorption and Fluorescence in toluene, ethanol, and acetonitrile	35
VIII.....Extinction coefficient in toluene	
36	
A. Experimental Stokes shift	36

B.	Excited-state-optimized and ground-state-optimized structure and orbital	37
C.	Fluorescence decay	38
D.	Quantum yield, Lifetime, and rate constant	41
IX.	Supplementary Information	42
A.	Compound appearance	42
B.	Solid spectrum of PTZ-NO₂	42
C.	Synthesis procedure	43
1.	Synthesis of PTZ-NO₂	43
2.	Synthesis of PTZ-NH₂	45
3.	Synthesis of PTZ-CHO	47
4.	Synthesis of PTZ-CN	49
5.	Synthesis of DPA-OMe	51
6.	Synthesis of PTZ-OMe	53
D.	Cyclic Voltammetry	55
1.	Cyclic Voltammetry graph	55
2.	HOMO LUMO energy	56
E.	Computational approach	57
1.	Ground state and excited state optimized structure	59
2.	Ground state optimized orbital	59
3.	Distance definition of r_C , $r_D +$, and $r_A -$	59
F.	Crystal data and structure refinement	60
1.	Crystallography of PTZ-OMe	60
2.	Crystallography of PTZ	62
3.	Crystallography of PTZ-CHO	64
4.	Crystallography of PTZ-NO₂	66





Content of Figure, Scheme, and Table

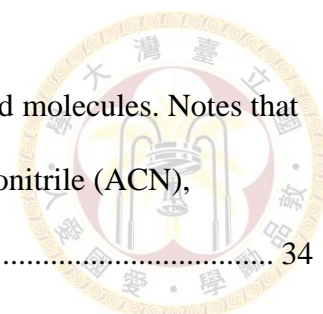


Figure 1. Normalized absorption and photoluminescence spectra of five entitled molecules. Notes that red, yellow, and green lines represent toluene (TOL), ethanol (EtOH), and acetonitrile (ACN), respectively.	34
Figure 2. Normalized absorption and photoluminescence spectra of five entitled molecules. Notes that orange, blue, and purple lines represent toluene (TOL), ethanol (EtOH), and acetonitrile (ACN), respectively.	35
Figure 3. Excited-state-optimized structure (1 st row), ground-state-optimized structure (2 nd row), as well as excited-state-optimized HOMO (3 rd row) and LUMO (4 th row) orbitals of the titled molecules computed by m062x/6-31+g(d,p) with cyclohexane as solvent.	37
Scheme 1. Chemical structures of phenothiazine and analogues modified at C3-position.	17
Scheme 2. Synthesis route of five entitled molecules.	18
Table 1. Excitation wavelength and standard dye of titled molecules	19
Table 2. Experimental and calculated optical characteristics for the titled molecules ^a	25
Table 3. Electrochemical properties and free energy of photoinduced electron transfer of the three entitled molecules with charge transfer.	28
Figure S1. Molar absorption coefficients of five entitled molecule measured in toluene.	36
Figure S2. Fluorescence decay spectrum of PTZ-OMe in five different solvent.	38
Figure S3. Fluorescence decay spectrum of PTZ in five different solvent.	38
Figure S4. Fluorescence decay spectrum of PTZ-CN in five different solvent.	39
Figure S5. Fluorescence decay spectrum of PTZ-CHO in five different solvent.	39

Figure S6. Fluorescence decay spectrum of PTZ-NO₂ in five different solvent.....	40
Figure S7. The appearance of entitled compounds under regular indoor light.	42
Figure S8. (a) Absorption spectra of PTZ-NO₂ in toluene (brown dash) and in 110 nm film made by vacuum deposition. Orange solid line is the PL spectrum of PTZ-NO₂ in s toluene. Green, Blue, and Purple dot lines are PL spectra of PTZ-NO₂ in solid film and powder form excited by different light source and collected by different detector. There are no meaningful peaks observed in solid PL spectrum of PTZ-NO₂ . No florescence when shine with hand-held UV light. (b) Appearance of PTZ-NO₂ in toluene. (c) Appearance of PTZ-NO₂ in 300 nm thick vacuum deposited film.	42
Figure S9. ¹ H NMR of PTZ-NO₂	44
Figure S10. ¹³ C NMR of PTZ-NO₂	44
Figure S11. ¹ H NMR of PTZ-NH₂	46
Figure S12. ¹³ C NMR of PTZ-NH₂	46
Figure S13. ¹ H NMR of PTZ-CHO	48
Figure S14. ¹³ C NMR of PTZ-CHO	48
Figure S15. ¹ H NMR of PTZ-CN	50
Figure S16. ¹³ C NMR of PTZ-CN	50
Figure S17. ¹ H NMR of DPA-OMe	52
Figure S18. ¹³ C NMR of DPA-OMe	52
Figure S19. 1H NMR of PTZ-OMe	54
Figure S20. 13C NMR of PTZ-OMe	54
Figure S21. Cyclic voltammograms of five entitled molecules. Reduction curves of PTZ derivatives are irreversible since they are easily oxidized.	55
Figure S22. Ground state and excited state optimized structure, with bending angle shown. Red plane was calculated from six carbons in the left benzene ring, green plane was calculated from six carbons in	

the right benzene ring, and the bending angle was defined as the smaller angle between red and green plane.	59
Figure S23. Ground state optimization of LUMO (upper) and HOMO (lower) orbitals for PTZ-OMe, PTZ, PTZ-CN, PTZ-CHO, and PTZ-NO ₂ in cyclohexane.	59
Figure S24. Ground state optimized structures in dichloromethane with the definition of <i>rc</i> , <i>rD</i> +, and <i>rA</i> -. A centroid of 22 atoms without the substituted group was calculated as D, the red sphere; another centroid of the substituted group was calculated as A, the green sphere. <i>rc</i> is the <i>DA</i> distance, <i>rD</i> + is the <i>DC3</i> distance, and <i>rA</i> - is the <i>C3A</i> distance.	59
Figure S25. X-ray crystal structure of PTZ-OMe	61
Figure S26. X-ray crystal structure of PTZ	63
Figure S27. X-ray crystal structure of PTZ-CHO	65
Figure S28. X-ray crystal structure of PTZ-NO₂	67
Scheme S1. Synthetic route of PTZ-NO₂	43
Scheme S2. Synthetic route of PTZ-NH₂	45
Scheme S3. Synthetic route of PTZ-CHO	47
Scheme S4. Synthetic route of PTZ-CN	49
Scheme S5. Synthetic route of DPA-OMe	51
Scheme S6. Synthetic route of PTZ-OMe	53
Table S1. Stokes shifts of five titled molecule in five different solvent a in unit of wavenumber calculated from the experimental peak wavelength of absorbance and photoluminescence spectrum.	36
Table S2. Excitation, monitoring wavelength as well as quantum yield, lifetime, and rate constate of the entitled molecules.	41

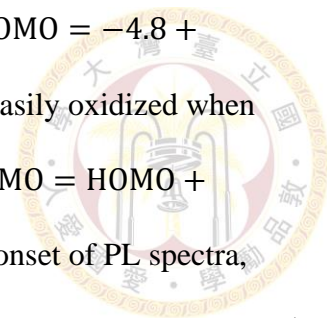


Table S3. HOMO LUMO energy calculated from CV and PL data. Usually, $HOMO = -4.8 + E_{oxiD} - E_{oxiFc}$ and $LUMO = -4.8 + E_{redA} - E_{redFc}$. However, **PTZ** is easily oxidized when measuring reduction potential, so the calculation of LUMO was adjusted as $LUMO = HOMO + EPL\ onset$, where *EPL onset* is the energy converted from the wavelength of onset of PL spectra, which is 420 nm is our case. 56

Table S4. Calculated wavelength (λ), oscillator strength (f) and orbital transition for five entitled molecules with m062x. 57

Table S5. Calculated wavelength (λ), oscillator strength (f) and orbital transition for five entitled molecules with b3lyp. 58

Table S5. Crystal data and experimental details for **PTZ-OMe**. 60

Table S6. Crystal data and experimental details for **PTZ**. 62

Table S7. Crystal data and experimental details for **PTZ-CHO**. 64

Table S8. Crystal data and experimental details for **PTZ-NO₂**. 66

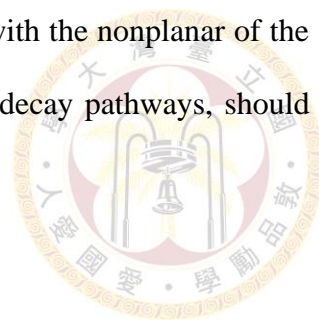
I. Introduction

Phenothiazine (**PTZ**) was first emerged in its derivative form, methylene blue, a medication as well as a dye that was prepared by Heinrich Caro in 1876 at BASF, a Germany-based European chemical company.^{1, 2} **PTZ** possesses a handful of biological activities and is widely known for its medical applications including insecticidal,² antifungal,³ antibacterial,⁴ and anthelmintic⁵ (expel parasitic worms and other internal parasites from the body) properties.

Phenothiazine (**PTZ**) has drawn great attention in both medical and optoelectronic fields since it was synthesized and characterized, and it has been used in a variety of aspects such as pharmaceutical chemistry,⁶⁻⁹ dye-sensitized solar cells (DSSCs),¹⁰⁻¹³ molecular designs in the thermally activated delayed fluorescence (TADF) molecules,¹⁴⁻¹⁸ organic light-emitting diode,¹⁹⁻²² and supramolecular host-guest system.^{23, 24} **PTZ** is known as an anthracene-shaped heterocyclic compound with electron-rich nitrogen and sulfur atom in the middle six-member ring (see **Scheme 1**). Therefore, owing to the electron sufficient sulfur atom, its electron density is more abundant than that of other heterocyclic compounds, such as phenoxazine, acridan and carbazole.^{18, 25} Moreover, **PTZ** could transform between three different states: neutral, cation radical (by losing an electron), and oxygenated sulfoxide state (by losing one more electron and double-bonding of sulfur atom to an oxygen atom) under suitable photoionization, providing another perspective in pharmaceutical fields.^{26, 27}

Such bio-synthetic versatility intrigues us to mull the potential of applying **PTZ** derivatives in luminescence-based bio-sensing. However, low photoluminescence quantum yields (PLQY) in both solution and solid of parent **PTZ** (PLQY = 0.16% in cyclohexane) and a number of **PTZ** derivatives were reported.^{28, 29} In sharp contrast, replacing sulfur in **PTZ** by the oxygen atom, forming phenoxazine (**POZ**), renders good to higher emission yield (PLQY = 2.7% in cyclohexane).³⁰ The result manifests the role of sulfur atom in harnessing the emission yield. The relatively soft sulfur atom may lift the energy of lone pair electrons. As a result, the $n\pi^*$ state is in close proximity to the $\pi\pi^*$ state in parent **PTZ**,

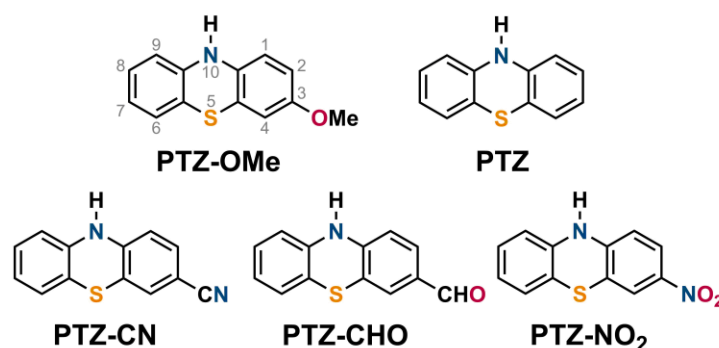
leading to the state mixing that reduces the transition moment. This, together with the nonplanar of the phenothiazine and hence the twisting motions that enhance the non-radiative decay pathways, should account for the low emission yield for **PTZ** (vide infra).



II. Motivation

In this study we report the design and syntheses of **PTZ** derivatives in an aim to harvest the emission in terms of yield and energy by harnessing the substituent at the **PTZ** moiety. Note that this approach is much distinct from the recent studies in which the whole **PTZ** moiety is used as an electron donating group to construct a D-bridge-A type thermally activated delay fluorescence (TADF) materials.^{14-17, 31} Realizing that sulfur long pair electron and twist along the sulfur-carbon bond play a key role, we intend to anchor various electron-withdrawing groups (EWG), including formyl (**-CHO**), cyano (**-CN**) and even nitro (**-NO₂**) functional groups at the *meta*- position with respect to the sulfur atom to lower the lone pair electron energy via the inductive effect. On the other hand, these EWG are intentionally added in the *para*- position of the phenothiazine nitrogen atom, rendering a potential for charge transfer (CT). We thus anticipate that the CT effect may lean the PTZ moiety toward a planar configuration to suppress the non-radiative twisting effect. For a fair comparison we also synthesized methoxy (**-OMe**) PTZ to represent the electron-donating group (EDG). As a result, the introduction of EDG and EWG reveals large effect on the luminescence properties, which are also supportive by the corresponding theoretical approaches. Remarkably, exploiting the **-NO₂** group that is conventionally thought to be good emission quencher, the **PTZ-NO₂** achieve 100% PLQY in nonpolar solvents. Detail of results and discussion are elaborated below.

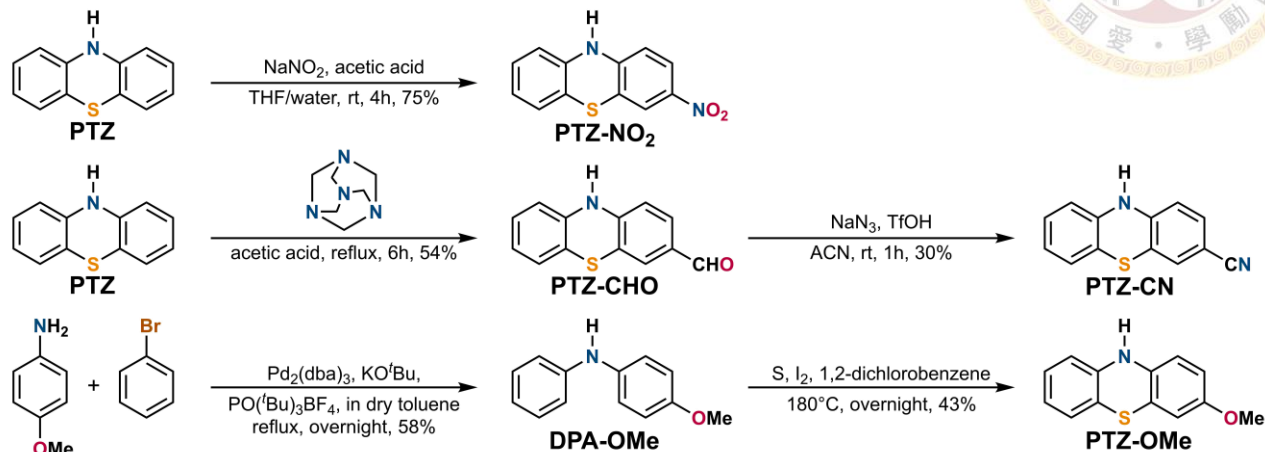
Scheme 1. Chemical structures of phenothiazine and analogues modified at C3-position.



III. Experiments

A. Synthesis

Scheme 2. Synthesis route of five entitled molecules.



Organic synthesis and NMR characterization was performed by my colleague, Yao-Lin Lee, who was a third-year doctoral student in our group as I wrote this thesis.

Firstly, **PTZ** was dissolved in THF and nitrated into **PTZ-NO₂** with concentrated sodium nitrite aqueous solution in ice bath.³² The nitro group were further reduced with active metal in an aqueous ethanol overnight to yield **PTZ-NH₂**. **PTZ-CHO** was synthesized through a Duff reaction, i.e., the hexamine aromatic formylation, by dissolving **PTZ** with hexamine in an acetic acid solution and reflux overnight.³³ Further, **PTZ-CHO** was converted to **PTZ-CN** via an improved Schmidt conversion³⁴ by dissolving purified **PTZ-CHO** with sodium azide in acetonitrile and add triflic acid during fast stirring. The synthesis of **PTZ-OMe** was performed from a mixture of 4-methoxyaniline and bromobenzene in dry toluene through a palladium-catalyzed coupling reaction to yield **DPA-OMe** (see **Scheme 2**),³⁵ which then underwent a ring-closure process by reacting with sulfur and iodine in 1,2-dichlorobenzene overnight to yield **PTZ-OMe**.³² All five titled compounds were characterized by ¹H and ¹³C NMR (see Synthesis procedure on p.43), and the appearance of five titled compounds were recorded in **Figure S7** (Compound appearance on p.42). Single crystal of selective compounds has been successfully obtained.



B. Absorbance

Prior to experiment, the double-beam spectrophotometer (U3310, manufactured by Hitachi) were turned on to allow the lamps to reach a stable condition. Two quartz cuvettes (dimension: 1×1×4.5 cm, manufactured by Purshee Experiment in China) were cleaned with acetone, dried by hair blower, and whipped with acetone-damped Kimwipe. In the sample compartment of, both reference slot and sample slot were placed with quartz cuvette, and filled with desired solvent to half-full. Parameters, set in Method section of the program, were configured to allow U3310 to scan from 900 nm to 300 nm at a 600 nm/min speed. After baseline, the pure solvent was measured without any modification to ensure the baseline correction is good. Then, the sample that were dissolved in desired solvent in advanced were added into the cuvette in the sample slot. The absorbances at intend excitation wavelength, as shown in **Table 1**, usually around the first absorption peak (longest in wavelength), were adjusted in a range of 0.10 to 0.11 for quantum yield analysis. For lifetime measurement and better absorption and photoluminescence spectrum, the absorbance was adjusted between 0.30 and 0.5.

Table 1. Excitation wavelength and standard dye of titled molecules

Titled molecule	Excitation wavelength (nm)	Standard dye (CAS #)
PTZ-NH₂, PTZ-OMe, PTZ	320	POPOP (1806-34-4)
PTZ-CN	380	C480 (171615-15-9)
PTZ-CHO, PTZ-NO₂	430	DCM (51325-91-8)

C. Photoluminescence

Before experiment, lamp and detector cooler of FS980 were turned on, slits were set at desired values, and suitable filter were selected to reduce second harmonic signal. Sample dissolved in desired solvent with reasonable concentration were placed in fluorescence spectrometer (FS980, manufactured by Edinburgh Instruments). Excitation wavelength were chosen at the peak wavelength of the first

absorption peak. For example, **PTZ** has its absorption spectrum peaks at 318 nm when using cyclohexane as solvent. Therefore, the concentration was adjusted at U3310 so that the absorbance at 320 nm is in a range of 0.10 to 0.11. In FS980, **PTZ** was excited at 320 nm, and scan from 310 nm to 630 nm, which included the excitation peak to ensure its correct, and 630 nm is 10 nm less than twice of the excitation wavelength to avoid second harmonic signal. To scan beyond 630 nm, a 380 nm long-pass filter was place between the sample and the detector to block the excitation light scatters onto the detector and generate second harmonic signal.

D. Quantum yield

The two common methods to measure quantum yield are integrating sphere method and comparative method, we adapted the latter one. Suitable standard dyes that possess emission at similar wavelength band to the sample were chosen, as shown in **Table 1**. The concentration of sample and dye were adjusted in a range of 0.10 to 0.11. The absorbance spectrum and photoluminescence spectrum of dye and sample were both measured on the same day under the same condition (temperature, slit, filter, etc.). The calculation of quantum yield is based on the following equation:

$$\frac{\phi_{(S)}}{Abs_{(S)} \cdot Area_{(S)} \cdot n_{(S)}^2} = \frac{\phi_{(R)}}{Abs_{(R)} \cdot Area_{(R)} \cdot n_{(R)}^2} \quad \text{Eq. 1}$$

, where ϕ is the quantum yield, Abs is the absorbance at the excitation wavelength, $Area$ is the integrated area of photoluminescence intensity to wavenumber (cm^{-1}), and n is the reflection index of the solvent used. The subscript (S) and (R) represent sample and reference dye, respectively. In Eq. 1, only $\phi_{(S)}$, the quantum yield of sample, is unknown, so it can be calculated.

E. Time-Correlated Single Photon Counting (TCSPC)

A 532 nm 80 MHz green pulse laser was generated by Millennia eV (manufactured by Spectra-Physics), a DPSS (diode-pumped solid-state) laser. The laser then passed through Tsunami (manufactured by Spectra-Physics), a flexible, high performance, ultrafast Ti:Sapphire oscillator, which offer the tuning range of 700 nm to 1080 nm. We used the 720 nm to generate the second harmonic frequency at 360 nm for the experiments in this work. 80 MHz of pulse laser only allow a measurement window of 12.5 ns; therefore, the 80 MHz 360 nm pulse laser then passed through Model 3980 (manufactured by Spectra-Physics), a pulse-selector that is able to reduce the frequency down to 8 MHz. Sample were dissolved in desired solvent with proper concentration (absorbance around 0.3 at excitation wavelength) and put into the sample holder. The laser passes through several adjusting mirrors and illuminate the sample. Emission was collected at a 90° angle with respect to the laser, and a 420 nm long-pass filter were placed between the sample and the detector. The detector was a MCP-PMT (microchannel plate photomultiplier tube), R3809U-50 (manufactured by Hamamatsu Photonics, assembled by Edinburgh Instruments). The collected data were fitted by Edinburgh's software.

F. Extinction coefficient

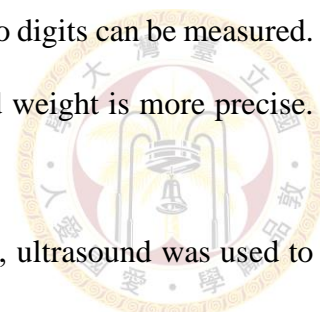
According to Beer-Lambert's law, absorbance (A) equals to the product of extinction coefficient (ϵ in $M^{-1}cm^{-1}$), cuvette length (b in cm), and concentration in (c in M), as shown in Eq. 2.

$$A = \epsilon b c \quad \text{Eq. 2}$$

Prior to experiment, a 20 ml volumetric flask was cleaned by soap water followed by acetone, and left dry in atmosphere. One can never dry volumetric container in an oven or use hair blower, since the heat will distort the glass and change the calibrated volumes.

A small amount (1.0 to 10.0 mg) of purified compound in powder form was weigh preciously in a 20 ml volumetric flask and dilute with desired solvent (toluene) to calibration line. The best electrical balance

in our lab has a readability of 0.1 mg; therefore, this step is critical since only two digits can be measured. If I use a larger volumetric flask (e.g. 200 ml), the measurement of compound weight is more precise. However, it cost 10.0 to 100.0 mg of compound to do this experiment. If compound hadn't fully dissolved when about 80% of the solvent was added, ultrasound was used to assist the dissolve process. Certain amount of solvent and compound solution were transferred into empty cuvette using micropipette of 100 μ L and 1000 μ L to achieve a dilution ratio of 1/21 and 1/31. The absorbance from several measurements were recorded, and an extinction coefficient of certain value can be calculated.



G. Thermal vapor deposition

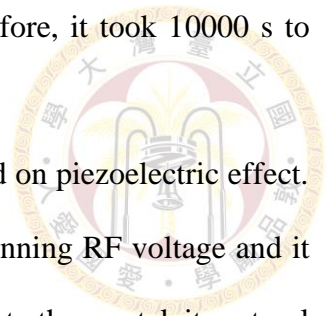
Thermal vapor deposition was performed by my colleague, Zhi-Xuan Huang, who was a first-year master student in our group as I wrote this thesis.

Six pieces of alkali-free glasses was cleaned ultrasonically; firstly, brush the glasses as vigorously as possible and then ultrasonicated with detergent water, acetone, isopropanol, deionized water sequentially and each for 20 min. Following the cleaning step, dry the cleaned glasses with strong nitrogen gas flow. Last, the glasses were treated with UV Ozone plasma for 15 min before vapor deposition.

The inner walls of vacuum deposition machine were covered with Al foil to prevent cross contamination. Approximately 10 mg of **PTZ-NO₂** powder was transferred to the cleaned quartz crucible as source material, which is then placed on the filament heater inside the chamber. Six pieces of alkali-free glasses were placed on the substrate rotor with a rate of 20 rpm. Vacuum environment was established by two-stage vacuum system. First stage is mechanical pump, which decreased the pressure down to 10⁻² torr or further, and turbo pump would turn on automatically to further reduce the pressure to 10⁻⁶ torr. After the desired vacuum is completed, Source substrate was heated by 20 amps of current at 1 volt, which heated the compound to 50°C. The deposition rate of such organic compound was usually range from 0.3 to 0.5

Å/s. To ensure packing stability, we set the deposition rate to 0.3 Å/s. Therefore, it took 10000 s to deposit a 300 nm film.

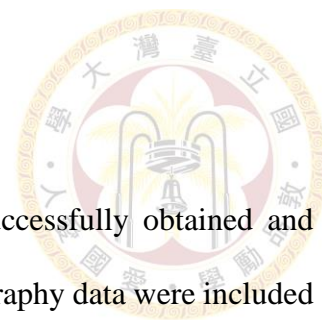
Thickness monitoring was fulfilled by quartz crystal resonator which was based on piezoelectric effect. A quartz crystal that were placed near the substrate was applied with a free-running RF voltage and it starts vibrating at its natural frequency. As more and more substrate deposited onto the crystal, its natural frequency decrease. This response can be modeled by a mathematical relationship, and the thickness of the sample substrate can be calculated.



IV. Results and Discussion

A. Structural Characterization

Single crystal of **PTZ-OMe**, **PTZ**, **PTZ-CHO**, and **PTZ-NO₂** has been successfully obtained and analyzed with Xcalibur, Atlas, Gemini ultra diffractometer. Detailed crystallography data were included in **SI** (See Crystal data and structure refinement on p. 60). The crystal of **PTZ-OMe** and **PTZ** are both monolithic with a space group of $P2_1/c$; the crystal of **PTZ-NO₂** and **PTZ-CHO** are both orthorhombic with a space group of $Pna2_1$. **PTZ-NO₂** has a Herringbone packing,³⁶ which indicates that there is a strong π - π interaction between different layers in solid state.



V. Solid state photophysical property of **PTZ-NO₂**

As shown in **Figure S28** (p. 67), the strong π - π interaction caused by the Herringbone packing absorbs a significant amount of light, making the solid powder appears to be black (**Figure S7** on p.42). Additionally, as shown in **Figure S8(c)** on p. 42, thin film of **PTZ-NO₂** made via thermal deposition appears to be purple, which corresponds to its solid absorbance peaks at 530 nm. Last, with in-built Xe light source or external laser, neither thin film or powder of **PTZ-NO₂** shows meaningful fluorescence peaks in visible and IR regime. Therefore, **PTZ-NO₂** is almost non-fluorescent in solid state.

Table 2. Experimental and calculated optical characteristics for the titled molecules ^a

Compound	Absorbance	Emission	Stokes shift	Quantum yields / Lifetime ^c (ns)		
	S ₀ →S ₁	S ₁ →S ₀	(cm ⁻¹)	k _r (s ⁻¹) / k _{nr} (s ⁻¹)		
	Peak ^b (nm) Exp./Cal.(f)	Peak ^b (nm) Exp./Cal.(f)	ΔE _{exp} ΔE _{calc}	CYH	TOL	DCM
PTZ-OMe	314 / 302 (0.0041)	448 / 426 (0.0084)	9526, 9690	0.29% / 0.38 7.56 × 10 ⁶ / 2.60 × 10 ⁹	0.42% / 0.75 5.63 × 10 ⁶ / 1.33 × 10 ⁹	0.56% / 2.33 2.40 × 10 ⁶ / 4.26 × 10 ⁸
PTZ	318 / 303 (0.0007)	433 / 420 (0.0080)	8352, 9211	0.16% / 0.74 2.16 × 10 ⁶ / 1.35 × 10 ⁹	0.24% / 0.86 2.80 × 10 ⁶ / 1.16 × 10 ⁹	0.22% / 0.81 2.73 × 10 ⁶ / 1.24 × 10 ⁹
PTZ-CN	331 / 323 (0.0741)	457 / 443 (0.0559)	8330, 8358	6.64% / 5.07 1.31 × 10 ⁷ / 1.84 × 10 ⁸	11.78% / 5.52 2.13 × 10 ⁷ / 1.60 × 10 ⁸	10.86% / 5.99 1.81 × 10 ⁷ / 1.49 × 10 ⁸
PTZ-CHO	376 / 340 (0.1248)	458 / 461 (0.0988)	4762, 7703	43.52% / 8.22 5.30 × 10 ⁷ / 6.87 × 10 ⁷	46.14% / 8.47 5.45 × 10 ⁷ / 6.36 × 10 ⁷	40.96% / 7.98 5.13 × 10 ⁷ / 7.39 × 10 ⁷
PTZ-NO₂	408 / 362 (0.1873)	522 / 496 (0.1694)	5353, 7474	100% / 7.63 1.31 × 10 ⁸ / 0.00 × 10 ⁰	29.08% / 2.76 1.06 × 10 ⁸ / 2.57 × 10 ⁸	0.54% / 0.24 2.29 × 10 ⁷ / 4.22 × 10 ⁹

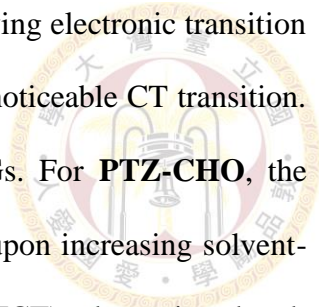
^a Experiments were conducted under room temperature, and calculation were performed with m062x/6-31+g(d,p) in cyclohexane. Exp. is the experimental lowest-lying absorption or emission wavelengths, Cal. is the calculated lowest-lying absorption or emission wavelengths, *f* represents oscillator strengths, ΔE_{exp} stands for experimental Stokes shift, ΔE_{calc} stands for calculated Stokes shift. ^b The experimental values are taken from the peak wavelength of the absorption and emission in cyclohexane in unit of nanometer. ^c Lifetime were measured by TCSPC and excited at 360 nm for all five compounds.

A. Photophysical properties

The steady-state absorption and emission spectra of the title compounds in three solvents, cyclohexane (CYH), toluene (TOL) and dichloromethane (DCM), are depicted in **Figure 1** (p. 34), and in other solvents, toluene (TOL), ethanol (EtOH), and acetonitrile (ACN), are depicted in **Figure 2** (p. 35). The selected photophysical properties are summarized in **Table 2** (p. 25), **Table S1** (p. 36), and **Table S2** (p. 41).

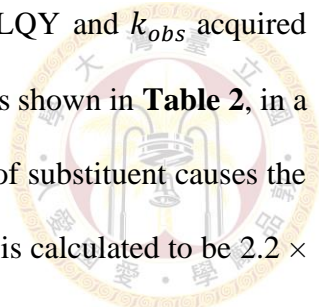
As shown in **Figure 1** (p. 34), the absorption peak of the EDG substituted **PTZ-OMe** around 320 nm can be ascribed to the π-π* transition of **PTZ** chromophore. Further, the emission peaks of **PTZ-OMe** are not varied by employing different polarity solvents and show mirror-imagined emission with respect to the lowest lying absorption band, affirming the locally excited (LE) emissive character with vibronic profile. Similar results can be observed in **PTZ** with absorption maximum at 320 nm and vibronic progressive emission maximized at 440 nm in all three solvents.

In sharp contrast, as substituted by the EWG at the C3-position, **PTZ-CN** shows a red-shifted absorption peak around 340 nm (cf. **PTZ**). By varying the solvent polarity, the emission peaks of **PTZ-CN** are observed at 450, 460 and 470nm in cyclohexane, toluene and dichloromethane solutions, respectively,



revealing solvatochromism effect. The result clearly indicates that the lowest lying electronic transition of **PTZ-CN** is no longer dominant by the LE transition but incorporates with noticeable CT transition. The observation is further supported by introducing formyl and nitro EWGs. For **PTZ-CHO**, the wavelength of the longest absorption tail (shoulder) is apparently red shifted upon increasing solvent-polarity, showing a typical character of intramolecular charge transfer (ICT) absorption band. Furthermore, the emission peaks are recorded at 470, 510, and 540 nm in cyclohexane, toluene, and dichloromethane solutions, respectively. More impressively, **PTZ-NO₂**, having its strongest electron withdrawing -NO₂ group, the emission band is red shifted from 540 nm in cyclohexane to as far as 700 nm in CH₂Cl₂, showing the most prominent excited-state ICT character. Hence, the strength of ICT effect of non-substituted and substituted **PTZ** analogies, based on the result of solvatochromism, is increased in the order of **PTZ-OMe** \approx **PTZ** < **PTZ-CN** < **PTZ-CHO** < **PTZ-NO₂**, which correlates well with the electron withdrawing strength of the substituent. The transformation from LE to CT character is further supported by the frontier orbital analyses elaborated in the section of computational approaches (vide infra).

The above results, though intriguing, may not be surprising in terms of interconversion between LE and CT states. What is even more important, to our viewpoint, is that the corresponding PLQY increases significantly from EDG to EWG substituted **PTZ**. For example, it is widely accepted that -NO₂ is a strong fluorescent quencher owing to its high energy level of nonbonding orbital with lone pair electrons (vide supra). To our surprise, however, PLQY of **PTZ-NO₂** is nearly 100% in the nonpolar solvents such as cyclohexane, which is in sharp contrast to the rather low PLQY for **PTZ** (0.16%) or **PTZ-OMe** (0.29%) in the same solvent (see **Table 2** on p. 25). To gain further insight, the fluorescence decay dynamics were measured by time-correlated single photon counting (TCSPC). The photoluminescence decays for all title compounds in various solvents are shown from **Figure S2** (p. 38) to **Figure S6** (p. 40) with pertinent data listed in **Table 2** (p. 25). As a result, PLQY can be expressed as $PLQY = k_r / k_{obs} = k_r / (k_r + k_{nr})$ where k_{obs} , k_r and k_{nr} denote the experimentally observed decay rate constant, the radiative decay rate



constant and the non-radiative decay rate constant, respectively. Combining PLQY and k_{obs} acquired experimentally, k_r and k_{nr} can thus be deduced and listed in **Table 2** (p. 25). As shown in **Table 2**, in a qualitative manner, it seems that increase of the electron withdrawing strength of substituent causes the increase of k_r but decrease of k_{nr} . For example, k_r of **PTZ** radiative decay rate is calculated to be $2.2 \times 10^6 \text{ s}^{-1}$, which is ~60 times as small as that of $1.3 \times 10^8 \text{ s}^{-1}$ in **PTZ-NO₂**. This, together with the largest k_{nr} of $1.3 \times 10^9 \text{ s}^{-1}$ for **PTZ** in cyclohexane, leads to its relatively much weaker emission compared with the **PTZ-EWG** molecules. In fact, k_r of $2.2 \times 10^6 \text{ s}^{-1}$ in **PTZ** manifests its forbidden-like lowest lying transition. Moreover, k_r increases as increasing the electron withdrawing strength (see **Table 2** on p. 25), indicating the more allowed lowest-lying transition. The results, on the one hand, implies increasing energy of the forbidden $n\pi^*$ character upon increasing the electron-withdrawing strength, proving the concept of lifting the $n\pi^*$ transition (vide supra) that is separated from the $\pi\pi^*$ state. On the other hand, in cyclohexane, the decrease of k_{nr} may imply the more planar of the **PTZ** moiety upon increasing the CT property. Support of these viewpoints is elaborated in the section of theoretical approach.

The above results and discussion are in the nonpolar solvent. In polar solvent, much decrease of PLQY for the **PTZ-EWG** molecules was observed upon increasing the solvent polarity (see **Table 2** on p. 25). Especially, for **PTZ-NO₂**, PLQY decreases from 100% in cyclohexane to 0.54 % in CH₂Cl₂. Knowing that emission of **PTZ-NO₂** has been red shifted to 700 nm, another non-radiative decay channel, i.e., the quenching of the S₁ electronic wave function by the overlap with ground-state high-frequency vibrational modes, is expected to be dominant. This so-called quenching rate operated by the energy gap law increases with decreasing energy gap, rendering the low PLQY in high polar solvent.³⁷⁻⁴⁰

B. Cyclic voltammetry analysis

Cyclic voltammetry (CV) analysis was also conducted to verify their intrinsic electronic properties, for which the corresponding CV diagram are shown in **Figure S21** on p. 55 and the numeric data are organized in **Table 3**. In the CV analysis, Ag/Ag⁺ (0.01M AgNO₃) electrode was selected as a reference electrode. The oxidation potentials were measured using a platinum (Pt) and glassy carbon electrode, respectively. Both experiments were conducted with 0.1 M of NBu₄PF₆ in dichloromethane and a gold wire with 0.1 M of NBu₄PF₆ in tetrahydrofuran as working electrode. The potentials were further referenced externally to the ferrocenium/ferrocene (Fc⁺/Fc) couple.

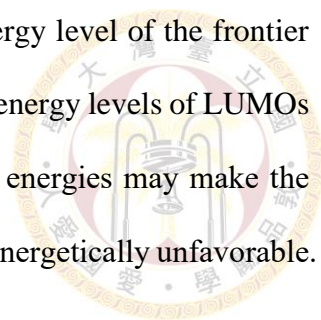
Table 3. Electrochemical properties and free energy of photoinduced electron transfer of the three entitled molecules with charge transfer.

Compound	E_{oxi}^D (V)	E_{red}^A (V)	HOMO (eV)	LUMO (eV)	ΔG kcal/mol
PTZ-OMe	0.49	-2.12	-4.80	-1.85	2.01
PTZ	0.63	-2.02	-4.94	-1.99	3.16
PTZ-CN	0.83	-2.12	-5.14	-2.19	-8.77
PTZ-CHO	0.80	-1.68	-5.12	-2.16	-13.69
PTZ-NO₂	0.84	-1.00	-5.16	-2.20	-21.22

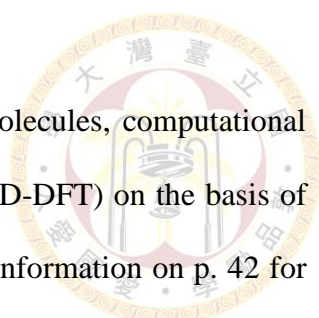
E_{oxi}^D and E_{red}^A are anodic and cathodic peak potentials using Fc⁺/Fc as reference. HOMO = $-(4.8 + E_{oxi}^D - E_{oxi}^{Fc})$ and LUMO = HOMO + E_{onset}^{PL} , where E_{onset}^{PL} is the energy converted from the wavelength of onset of PL spectra, which is 420 nm is our case. Free energy, ΔG_{PET} , is calculated by the following equation based on Marcus theory.

As tabulated in **Table 3**, the recorded HOMO are gradually shifted to the more negative side in an order of **PTZ-OMe** (-4.8 eV) > **PTZ** (-4.9 eV) > **PTZ-CN** (-5.1 eV) \approx **PTZ-CHO** (-5.1 eV) > **PTZ-NO₂** (-5.2 eV), which is consistent with the overall trend of electron donor capability (EDG > non-substituted > EWG). Moreover, as we computed the energy levels of LUMOs by adding the energy gap of the absorption onset, we obtained the associated values in an order of **PTZ-OMe** (-1.50 eV) > **PTZ** (-1.53 eV) > **PTZ-CN** (-2.30 eV) > **PTZ-CHO** (-2.48 eV) > **PTZ-NO₂** (-2.84 eV) as shown in **Table 3**, which was correlated (in a reverse manner) with the sequence of the HOMO and electron donor capability. In this regard; on the one hand, CV analysis verifies our observation from computational approaches (vide

supra) and gives a direct evidence that the EWGs strongly lower down the energy level of the frontier orbitals in the substituted aromatic ring. On the other hand, the modifications in energy levels of LUMOs are believed to have a major effect to the π^* orbitals, in which the decreased energies may make the mixing of nonbonding orbitals of sulfur atom and π orbitals of the aromatic ring energetically unfavorable.



C. Computational approaches



To gain in-depth insight into the electronic transition character of the title molecules, computational approaches were conducted using time-dependent density functional theory (TD-DFT) on the basis of m062x functional associated with 6-31+G(d,p) basis sets (see Supplementary Information on p. 42 for details). Although b3lyp is more widely accepted for calculation of charge transfer cases, the absorbance and emission wavelength calculated with m062x shown less deviation from the experimental result. Thus, we provided the result of m062x in manuscript, and attached the results of both m062x and b3lyp in the SI. The computed energy gaps and the associated frontier orbitals are recorded in **Table 2** (p. 25) and **Figure 3** (p. 37). After geometric optimization in their ground states (S_0), the title molecules all exhibit a bending type geometry owing to the existence of the electron-sufficient sulfur atom as shown in **Figure 3**. However, as we defined the bending angle (θ) as the angle intercepted by the two planes averaged from the six carbons on both side of the six-membered ring of phenothiazine, there exists a trend toward planarization in ground state optimized structure, which the angle is in the order of **PTZ-OMe** > **PTZ** > **PTZ-CN** \approx **PTZ-CHO** > **PTZ-NO₂**. The EWG reduce the electron density on sulfur atom, which decrease the size of its lone-pair, causing the bending angle to decrease. Moreover, the highest occupied molecular orbitals (HOMOs) of the title molecules are mainly localized at the middle of **PTZ** core as shown in **Figure S22** on p. 59.

With an aim to investigate their emissive properties, we then conducted the geometric optimization in their lowest lying excited state (S_1), their relative structural characters and frontier orbitals are shown in **Figure 3** (p. 37) and **Figure S22** to **Figure S24** (p. 59), respectively.⁴¹ As shown in **Figure 3**, the lowest unoccupied molecular orbitals (LUMOs) of the EDG substituted **PTZ-OMe** and parent **PTZ** are still mainly localized on the **PTZ** main core, revealing a LE transition character. More importantly, the contribution of the nonbonding orbitals from the sulfur atom is non-negligible in their LUMOs. The

results indicates that the lowest lying transition contains $\pi\pi^*$ overlapping with certain degrees of non-bonding character from sulfur atom.⁴² In sharp contrast, upon introducing EWGs on **PTZ**, the energy level of the substituted aromatic rings decreases, resulting in the lower energy of HOMO compared with the non-substituted **PTZ**. From another perspective, the EWGs make the substituted six-membered ring mainly contributing to LUMOs, diminishing the mixing between $\pi\pi^*$ and $n\pi^*$ states. Accordingly, LUMOs of EWG substituted analogies (**PTZ-CN**, **PTZ-CHO** and **PTZ-NO₂**) are mainly ascribed to the substituted functional groups; the net results reveal CT character.

Combine the above results, the rationalization of the transformation from LE to CT character may be offered in a quantitative manner based on the Marcus-Weller equation expressed below (eq. 1) to deduce the associated free energy (ΔG) of charge transfer in the excited state.⁴³ The equation is listed below:

$$\Delta G = E_{oxi}^D - E_{red}^A - E_{00} - \left(\frac{e^2}{4\pi\epsilon_0\epsilon_s r_c} \right) - \left(\frac{e^2}{8\pi\epsilon_0} \right) \left(\frac{1}{r_{D+}} + \frac{1}{r_{A-}} \right) \left(\frac{1}{\epsilon_{DCM}} - \frac{1}{\epsilon_s} \right) \text{ (eq. 1)}$$

where $E_{oxi}(D)$ and $E_{red}(A)$ are the oxidative and reductive potential, respectively, measured by cyclic voltammetry; E_{00} are recorded from the 0-0 transition of the title molecules where charge transfer process start to take place; ϵ_0 , ϵ_s , and ϵ_{DCM} are dielectric constants in vacuum, desired solvent and dichloromethane, respectively; r_c are recorded the distance between donor and acceptor; r_{D+} and r_{A-} are the ionic radii of donor and acceptor, respectively. The definitions of r_c , r_{D+} , and r_{A-} are visually shown in **Figure S24** (p. 59). Though it is not common to adapt this equation that were originally designed for photoinduced electron transfer (PET) to our charge transfer (CT) case, we found the result quiet convincing.

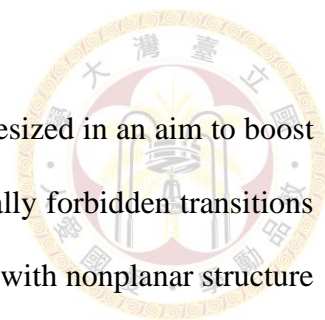
Employing all the recorded values to eq. 1. The corresponding ΔG for undergoing charge transfer are recorded in **Table 3** on p. 28. Accordingly, ΔG for the title molecules are in the order of **PTZ** (3.16 kcal/mol) > **PTZ-OMe** (2.01 kcal/mol) > **PTZ-CN** (-8.77 kcal/mol) > **PTZ-CHO** (-13.69 kcal/mol) > **PTZ-NO₂** (-21.22 kcal/mol). It is thus reasonable to expect that the exergonicity of the title molecules undergoing charge transfer follow the order of **PTZ-OMe** \approx **PTZ** < **PTZ-CN** < **PTZ-CHO** < **PTZ-NO₂**.

Additionally, it is worth to note that the uncertainty of this assessment should be appreciable in recording the emissive energy gap in solution and CV potentials. Also, the definition of r_{D^+} and r_{A^-} is ambiguous, which is only localized at the donor and acceptor sites. Nevertheless, **PTZ-OMe** and **PTZ** show positive ΔG , which indicates that the CT process is thermodynamically unfavorable, consisting with their LE emission concluded experimentally. On the contrary, the experimentally estimated ΔG of the EWG substituted **PTZ** analogies are all negative, indicating the accessibility of charge transfer process and resulting the CT emission. The trend of the exergonicity correlates with the experimental results.

Last but not the least, it is worth to note that upon geometric optimization in their excited states, **PTZ** core may undergo certain degrees of excited state structural planarization to enhance its π -conjugation, which is a general observation in **PTZ** and other heterocyclic derivatives such as phenazine.⁴¹ Accordingly, the more planar configuration upon increasing the electron withdrawing group (see **Figure S22** on p. 59) gives less twisted motion, and hence the decrease of non-radiative decay rate, rationalizing the ~100% PLQY for **PZT-NO₂** in the nonpolar solvent.

VI. Conclusion

In conclusion, a series of **PTZ** analogies were strategically designed and synthesized in an aim to boost the emission intensity. **PTZ** and the EDG substituted **PTZ-OMe** exhibit partially forbidden transitions because their π^* are mixed with nonbonding orbitals on S atom. This, together with nonplanar structure that activates the twisting non-radiative deactivation, rationalizes their weak emission. Conversely, introducing EWGs lowers the energy level of LUMO and diminish the mixing of nonbonding orbitals to facilitate the allowed π - π^* transition. Also, the EWGs substitution induces excited-state charge transfer, which suppresses the twisting non-radiative deactivation to enhance the emission. Among them, a widely considered fluorescent quencher functional group ($-\text{NO}_2$) was also employed in this work. **PTZ-NO₂** exhibits brilliant photophysical properties with 100% Q.Y. in nonpolar solvents (e.g., cyclohexane), which also shows significant solvatochromism in polar solvents, covering the visible region from 500 to 700 nm.



VII. Spectra, computed frontier orbitals, and additional tables



A. Absorption and Fluorescence in cyclohexane, toluene and dichloromethane

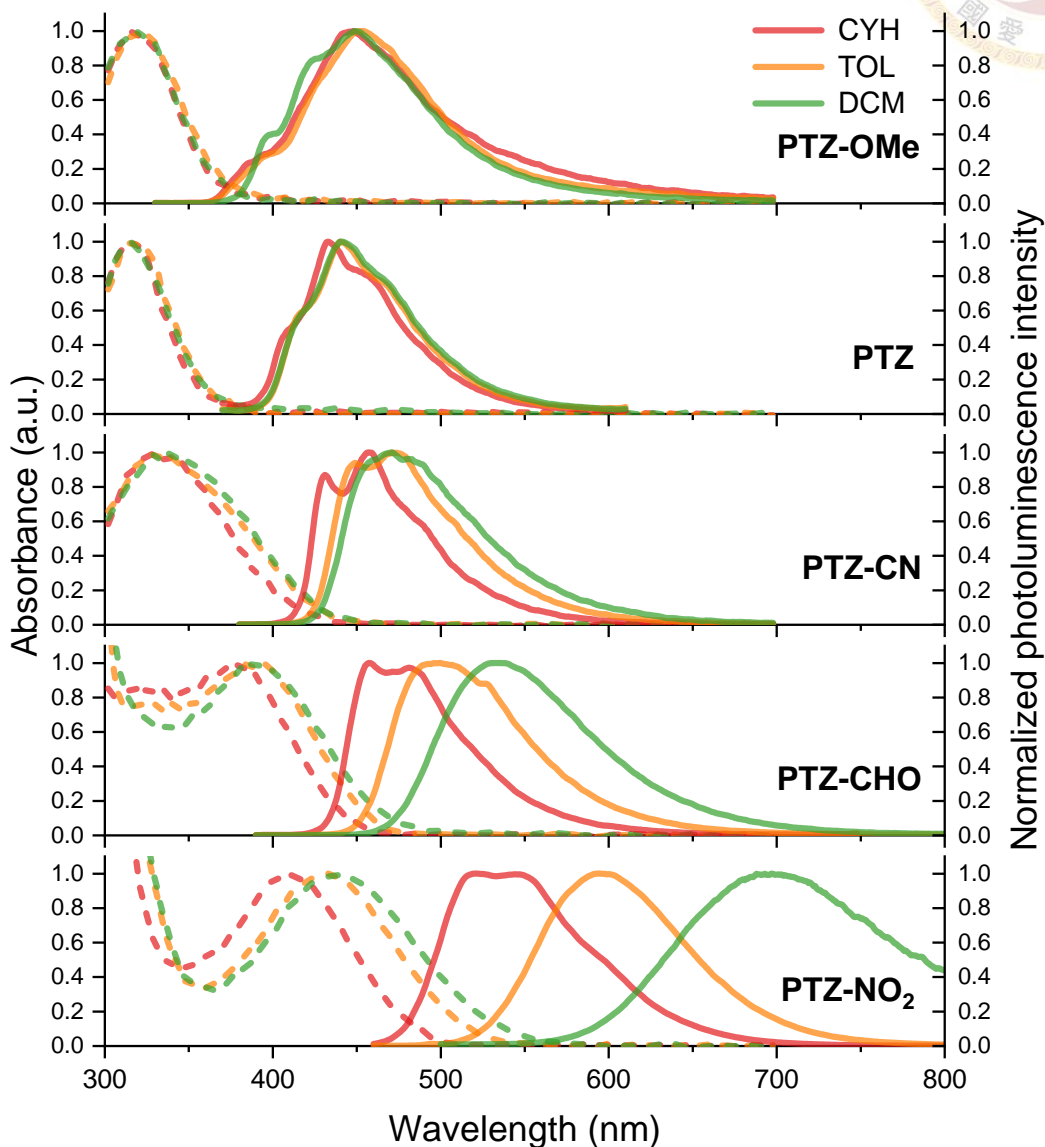


Figure 1. Normalized absorption and photoluminescence spectra of five entitled molecules. Notes that red, yellow, and green lines represent toluene (TOL), ethanol (EtOH), and acetonitrile (ACN), respectively.

B. Absorption and Fluorescence in toluene, ethanol, and acetonitrile

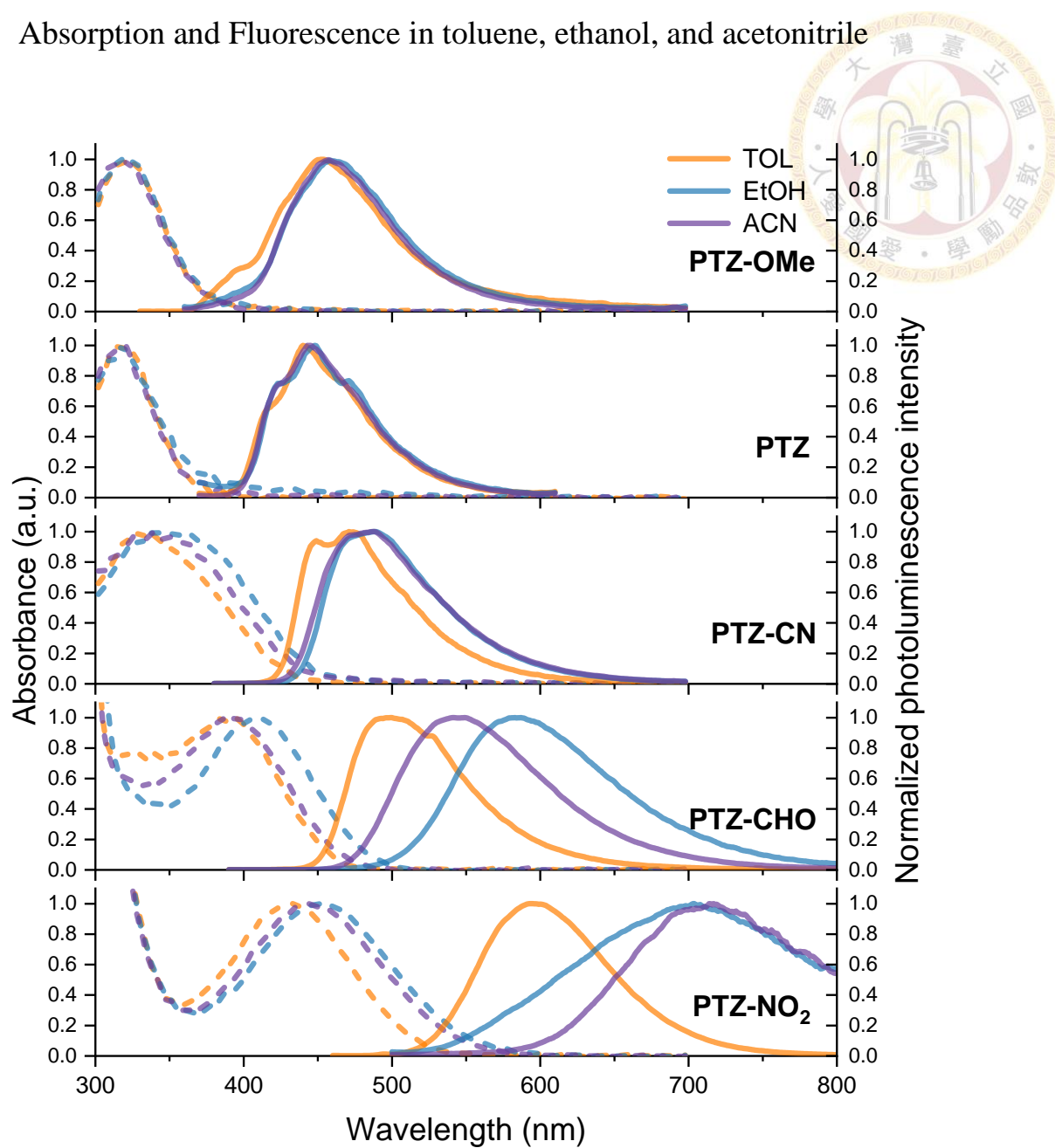


Figure 2. Normalized absorption and photoluminescence spectra of five entitied molecules. Notes that orange, blue, and purple lines represent toluene (TOL), ethanol (EtOH), and acetonitrile (ACN), respectively.

VIII. Extinction coefficient in toluene

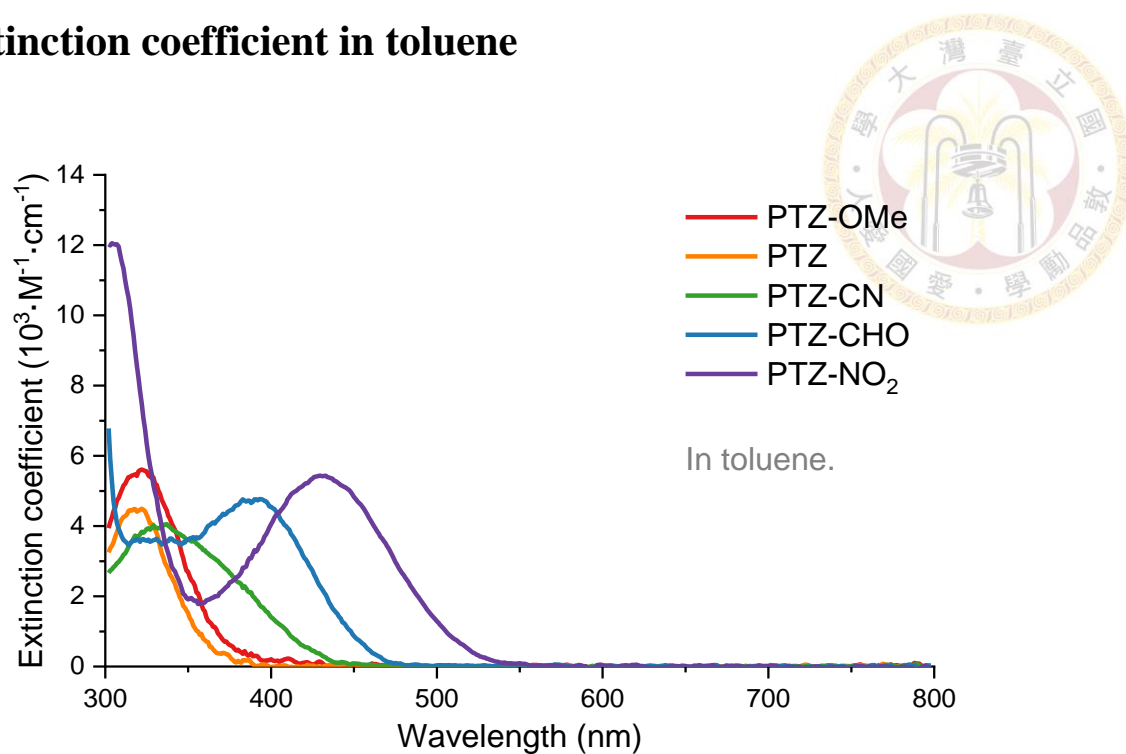


Figure S1. Molar absorption coefficients of five entitied molecule measured in toluene.

A. Experimental Stokes shift

Table S1. Stokes shifts of five titled molecule in five different solvent a in unit of wavenumber calculated from the experimental peak wavelength of absorbance and photoluminescence spectrum.

Abs./PL (nm) Stokes shift (cm ⁻¹)	CYH	TOL	DCM	EtOH	ACN
PTZ-OMe	314, 448 9526	322, 453 8981	317, 449 9274	318, 459 9660	317, 457 9664
PTZ	318, 433 8352	319, 441 8672	313, 441 9273	318, 448 9125	319, 445 8876
PTZ-CN	331, 457 8330	334, 472 8754	339, 471 8267	346, 489 8452	341, 487 8792
PTZ-CHO	376, 458 4762	390, 498 5561	388, 531 6941	409, 587 7414	394, 549 7166
PTZ-NO₂	408, 522 5353	430, 595 6449	440, 697 8380	449, 712 8227	444, 711 8458

CYH = cyclohexane, TOL = toluene, DCM = dichloromethane (DCM), EtOH = ethanol (EtOH), and ACN = acetonitrile.

B. Excited-state-optimized and ground-state-optimized structure and orbital

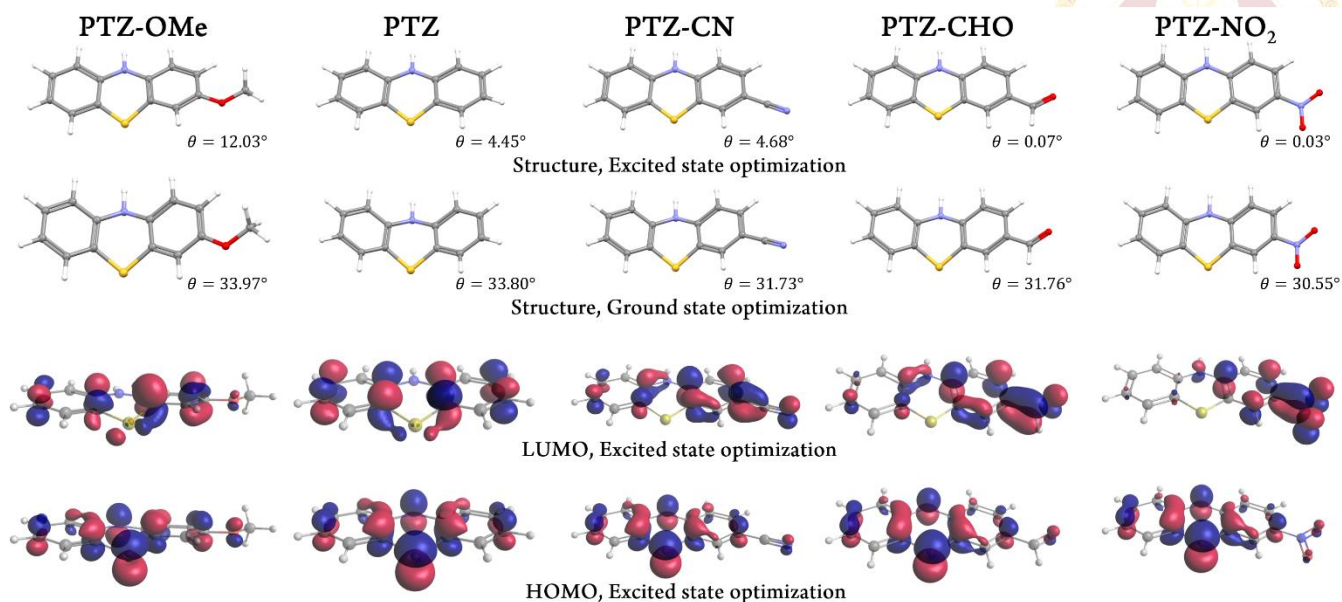


Figure 3. Excited-state-optimized structure (1st row), ground-state-optimized structure (2nd row), as well as excited-state-optimized HOMO (3rd row) and LUMO (4th row) orbitals of the titled molecules computed by m062x/6-31+g(d,p) with cyclohexane as solvent.

C. Fluorescence decay



PTZ-OMe

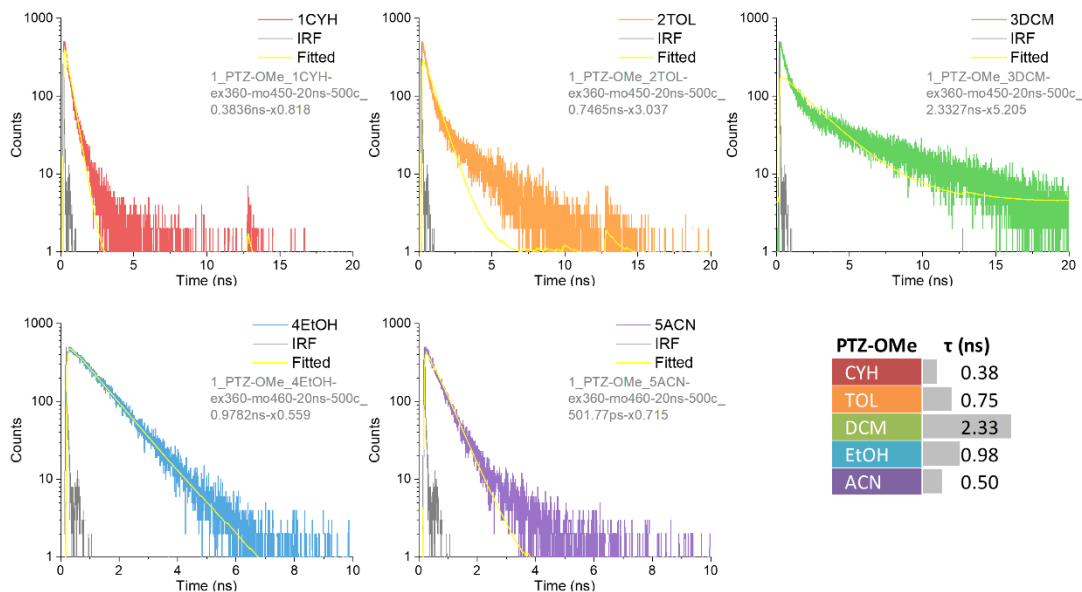


Figure S2. Fluorescence decay spectrum of PTZ-OMe in five different solvent.

PTZ

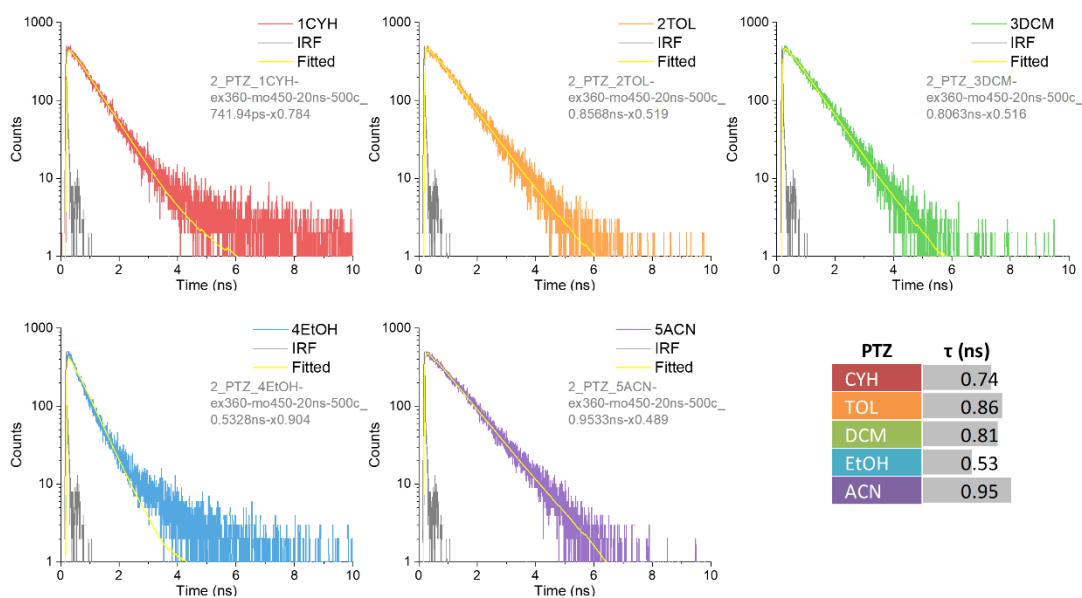


Figure S3. Fluorescence decay spectrum of PTZ in five different solvent.

PTZ-CN

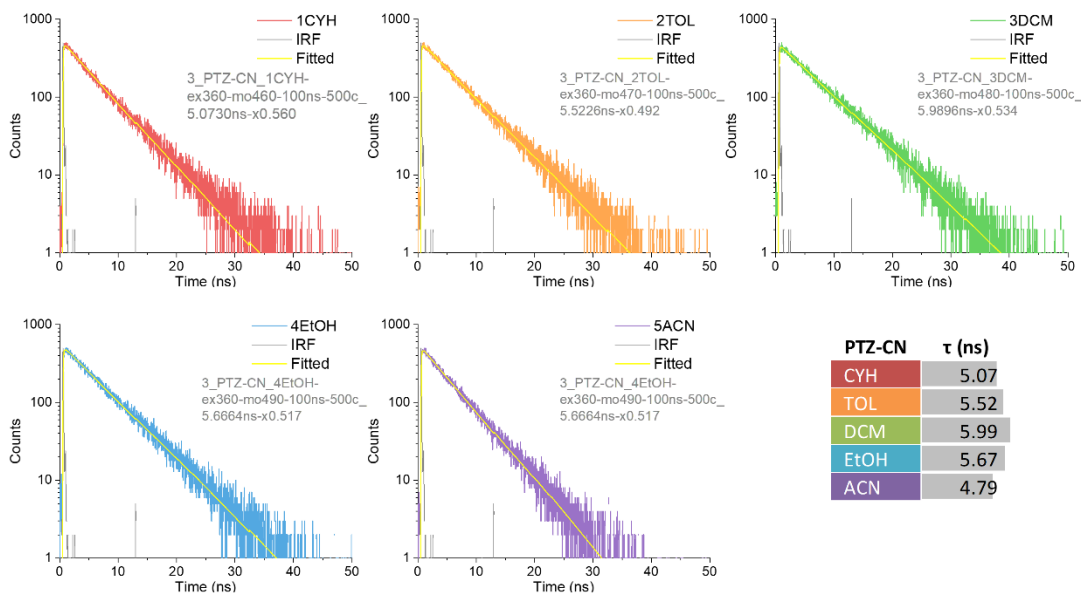


Figure S4. Fluorescence decay spectrum of PTZ-CN in five different solvent.

PTZ-CHO

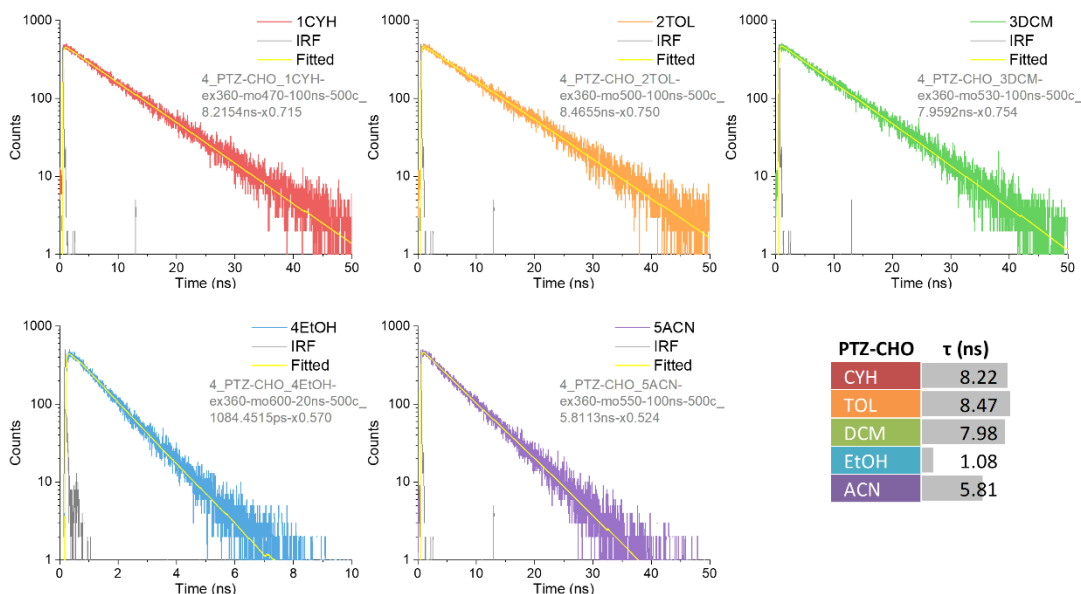


Figure S5. Fluorescence decay spectrum of PTZ-CHO in five different solvent.

PTZ-NO₂

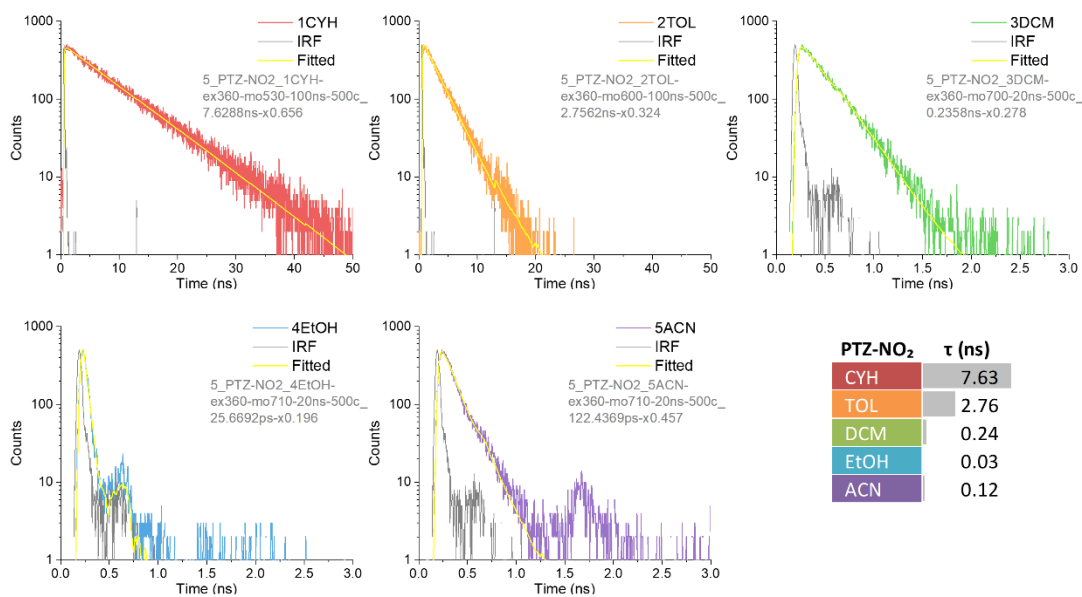


Figure S6. Fluorescence decay spectrum of PTZ-NO₂ in five different solvent.

D. Quantum yield, Lifetime, and rate constant

Table S2. Excitation, monitoring wavelength as well as quantum yield, lifetime, and rate constant of the entitled molecules.

Compound	Solvent ^a	Ex./Mon. ^b (nm)	Q.Y. ^c (%)	Lifetime ^d (ns)	k_r (s ⁻¹) ^e	k_{nr} (s ⁻¹) ^f
PTZ-OMe	CYH	320 / 450	0.29	0.38	7.56×10^6	2.60×10^9
	TOL	320 / 450	0.42	0.75	5.63×10^6	1.33×10^9
	DCM	320 / 450	0.56	2.33	2.40×10^6	4.26×10^8
	EtOH	320 / 460	0.26	0.98	2.66×10^6	1.02×10^9
	ACN	320 / 460	0.27	0.50	5.38×10^6	1.99×10^9
PTZ	CYH	320 / 450	0.16	0.74	5.63×10^6	1.33×10^9
	TOL	320 / 450	0.24	0.86	2.40×10^6	4.26×10^8
	DCM	320 / 450	0.22	0.81	2.66×10^6	1.02×10^9
	EtOH	320 / 450	0.51	0.53	5.38×10^6	1.99×10^9
	ACN	320 / 450	0.48	0.95	2.16×10^6	1.35×10^9
PTZ-CN	CYH	320 / 460	6.64	5.07	2.40×10^6	4.26×10^8
	TOL	320 / 470	11.78	5.52	2.66×10^6	1.02×10^9
	DCM	320 / 480	10.86	5.99	5.38×10^6	1.99×10^9
	EtOH	320 / 490	14.97	5.67	2.16×10^6	1.35×10^9
	ACN	320 / 490	11.64	4.79	2.80×10^6	1.16×10^9
PTZ-CHO	CYH	380 / 470	43.52	8.22	2.66×10^6	1.02×10^9
	TOL	380 / 500	46.14	8.47	5.38×10^6	1.99×10^9
	DCM	380 / 530	40.96	7.98	2.16×10^6	1.35×10^9
	EtOH	380 / 600	6.48	1.08	2.80×10^6	1.16×10^9
	ACN	380 / 550	35.42	5.81	2.73×10^6	1.24×10^9
PTZ-NO₂	CYH	430 / 530	100	7.63	5.38×10^6	1.99×10^9
	TOL	430 / 600	29.08	2.76	2.16×10^6	1.35×10^9
	DCM	430 / 700	0.54	0.24	2.80×10^6	1.16×10^9
	EtOH	430 / 710	0.14	0.03	2.73×10^6	1.24×10^9
	ACN	430 / 710	0.35	0.12	9.57×10^6	1.87×10^9

^a CYH = cyclohexane, TOL = toluene, DCM = dichloromethane (DCM), EtOH = ethanol (EtOH), and ACN = acetonitrile. ^b Ex. is the excitation wavelength for measuring quantum yield. Mon. is the monitoring wavelength when measuring lifetime. ^c Q.Y. is the quantum yield measured comparatively with POPOP, C480, and DCM as standard dye. ^d Lifetime were measured with TCSPC and excited at 360 nm for all five compounds. ^e k_r is radiative decay rate constant. ^f k_{nr} is non-radiative decay rate constant.

IX. Supplementary Information



A. Compound appearance

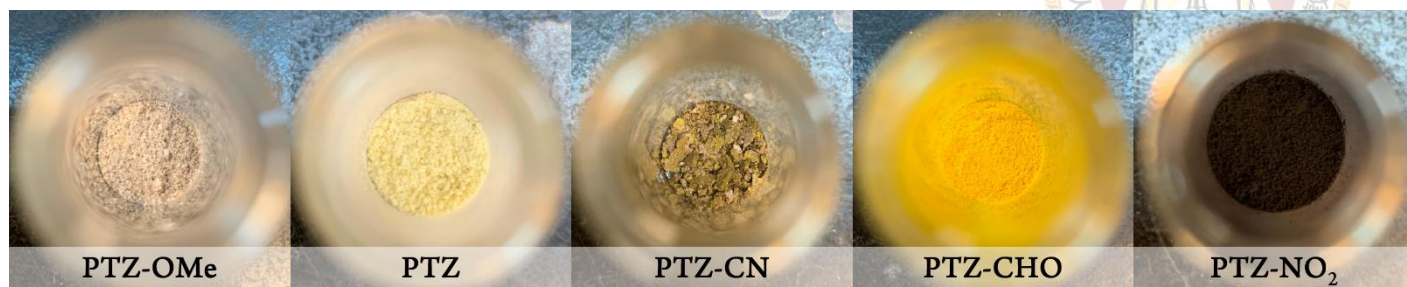


Figure S7. The appearance of entitled compounds under regular indoor light.

B. Solid spectrum of **PTZ-NO₂**

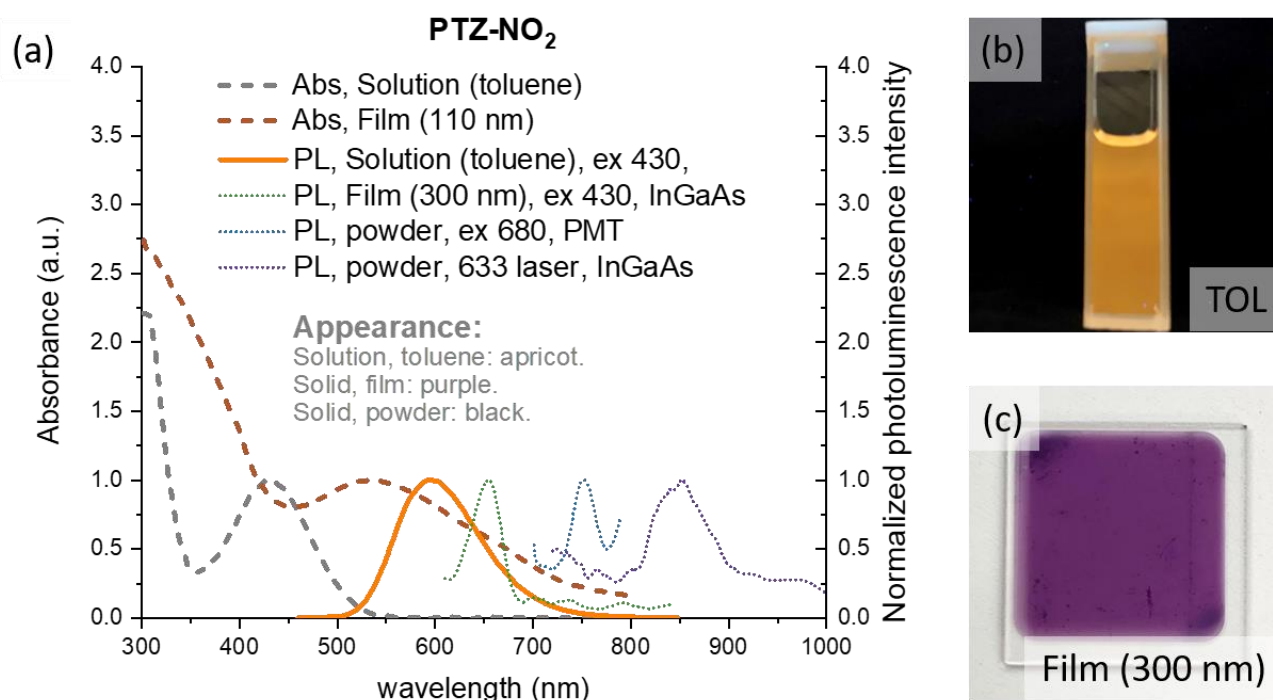
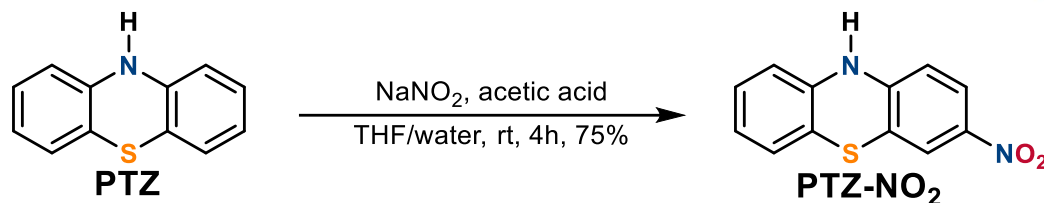


Figure S8. (a) Absorption spectra of **PTZ-NO₂** in toluene (brown dash) and in 110 nm film made by vacuum deposition. Orange solid line is the PL spectrum of **PTZ-NO₂** in s toluene. Green, Blue, and Purple dot lines are PL spectra of **PTZ-NO₂** in solid film and powder form excited by different light source and collected by different detector. There are no meaningful peaks observed in solid PL spectrum of **PTZ-NO₂**. No florescence when shine with hand-held UV light. (b) Appearance of **PTZ-NO₂** in toluene. (c) Appearance of **PTZ-NO₂** in 300 nm thick vacuum deposited film.

C. Synthesis procedure

1. Synthesis of **PTZ-NO₂**

Scheme S1. Synthetic route of **PTZ-NO₂**.



To the solution of phenothiazine (1 g, 5.02 mmole, 1 equiv.) in the THF (5 ml) and acetic acid (1.5 ml) in the ice bath was added a concentrated solution of sodium nitrite (1.08 g, 15.06 mmole, 3 equiv.) in water (2 ml) dropwise and stirred in the room temperature overnight. After completion of reaction, the reactant was extracted by ethyl acetate and brine. The organic layer was separated, dried over the MgSO_4 and concentrated by rotavapor. The crude product could be purified by silica column (ethyl acetate: hexane = 1: 3 with 1% TEA). The pure product **PTZ-NO₂** was black powder (3.75 mmole, 0.915 g, 75 %) mp = 182°C, FT-IR (cm^{-1}): 3475, 3318, 1567, 1537, 1326, 734. ^1H NMR (400 MHz, DMSO) δ 9.51 (s, 1H), 7.85 (d, J = 11.4 Hz, 1H), 7.73 (s, 1H), 7.02 (t, J = 7.6 Hz, 1H), 6.93 (d, J = 7.7 Hz, 1H), 6.84 (t, J = 8.0 Hz, 1H), 6.69 (d, J = 8.9 Hz, 2H). ^{13}C NMR (101 MHz, DMSO) δ 147.75, 140.97, 138.79, 128.16, 126.27, 124.68, 123.66, 121.60, 116.92, 115.41, 115.25, 113.35. HRMS (ESI-TOF) m/z: $[\text{M}+\text{H}]^+$ Calc'd for $\text{C}_{12}\text{H}_8\text{N}_2\text{O}_2\text{S}$ [245.03]; Found 245.03.

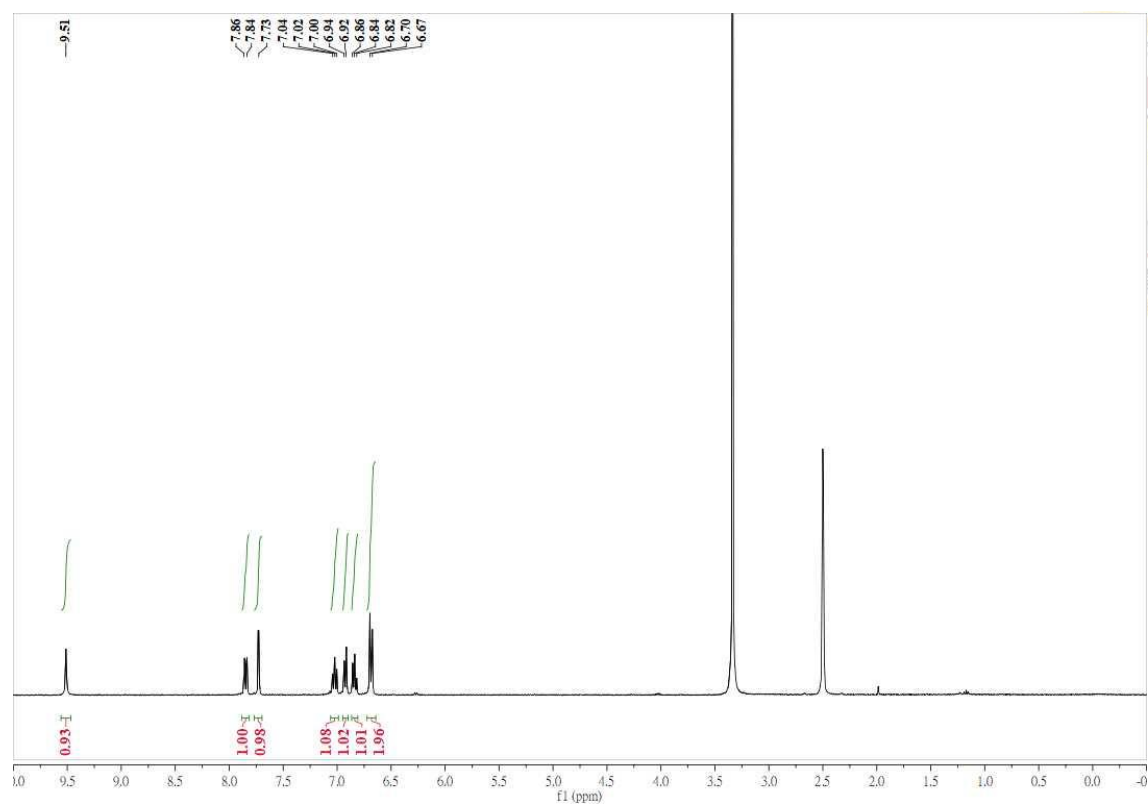


Figure S9. ^1H NMR of PTZ-NO₂.

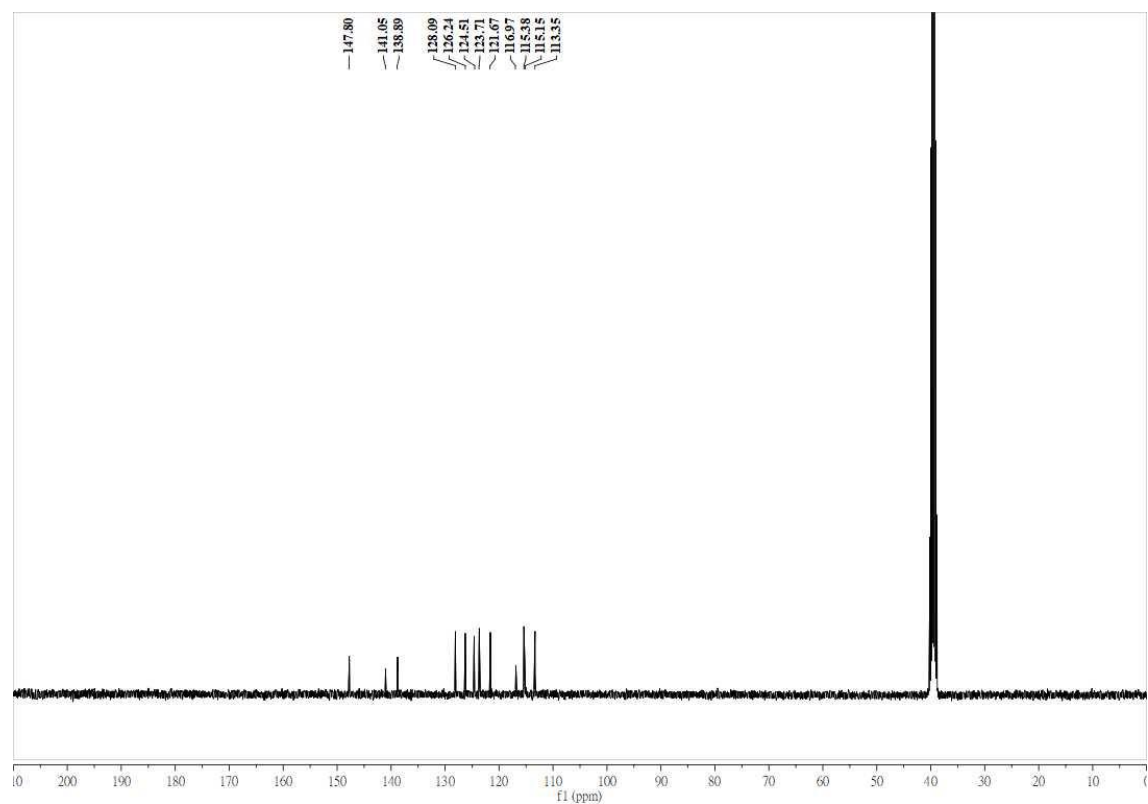
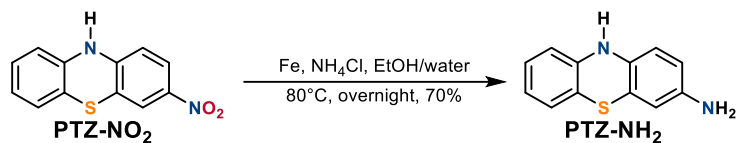


Figure S10. ^{13}C NMR of PTZ-NO₂.

2. Synthesis of **PTZ-NH₂**

Scheme S2. Synthetic route of **PTZ-NH₂**.



To the solution of 3-nitrophenothiazine (0.3g, 1.23mmole, 1equiv.) in the ethanol 12 ml and water (3ml), Fe (0.69g, 12.3mmole, 10equiv.) and NH₄Cl (0.26g, 4.92mmole, 4equiv.) were added. The system was heated to 80°C and reacted for 6 hours. After completion of reaction, the reaction solution was evaporated by rotavapor and then extracted with ethyl acetate and brine. The organic layer was separated, dried over MgSO₄ and concentrated by rotavapor. The crude product could be purified by silica column (ethyl acetate: hexane= 1: 1). The pure product **PTZ-NH₂** was black powder (0.184g, 0.86mmole, 70%). mp = 134-136°C. FT-IR (cm⁻¹): 3436, 2063, 1638, 1475, 1315, 739. ¹H NMR (400 MHz, DMSO) δ 8.08 (s, 1H), 7.00 – 6.91 (m, 1H), 6.87 (d, J = 9.1 Hz, 1H), 6.67 (d, J = 7.5 Hz, 1H), 6.62 (d, J = 7.9 Hz, 1H), 6.44 (d, J = 8.3 Hz, 1H), 6.31 – 6.18 (m, 2H), 4.65 (s, 2H). ¹³C NMR (101 MHz, DMSO) δ 143.77, 143.34, 131.72, 127.22, 126.10, 120.60, 116.80, 116.02, 115.15, 113.91, 113.20, 111.67. m/z: [M+H]⁺ Calc'd for C₁₂H₈N₂O₂S [214.06]; Found 214.06.

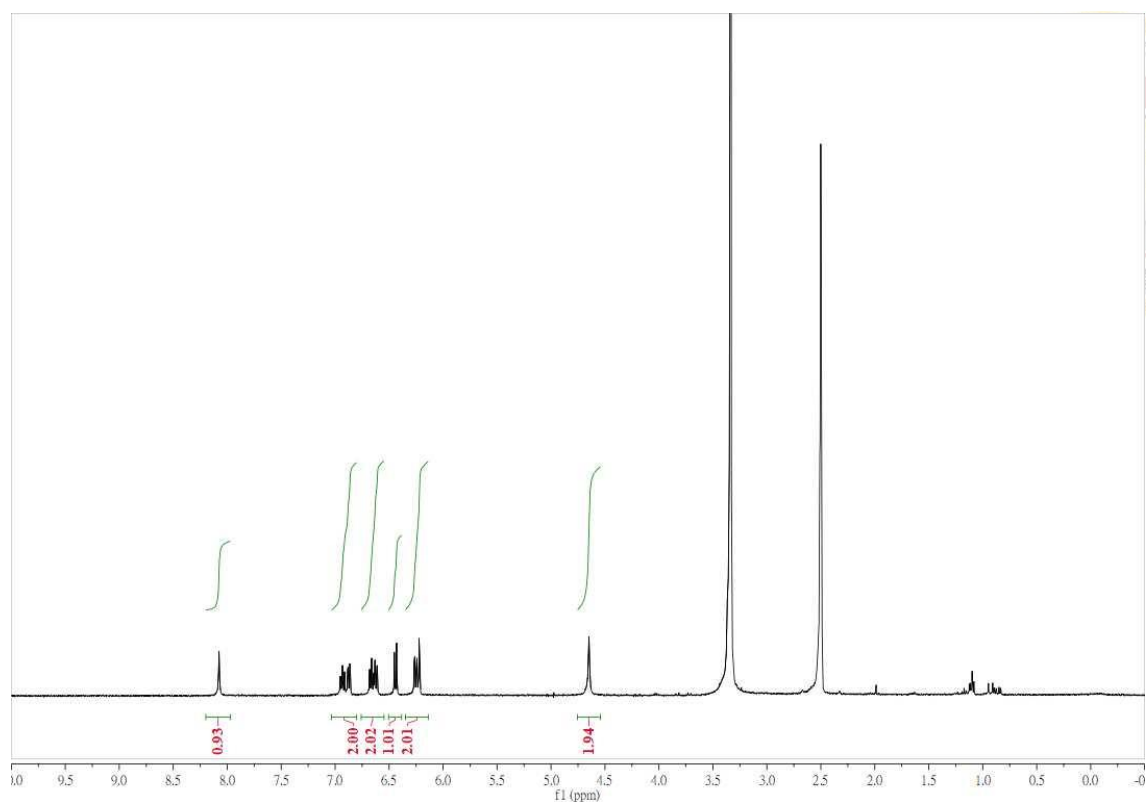


Figure S11. ^1H NMR of PTZ-NH₂.

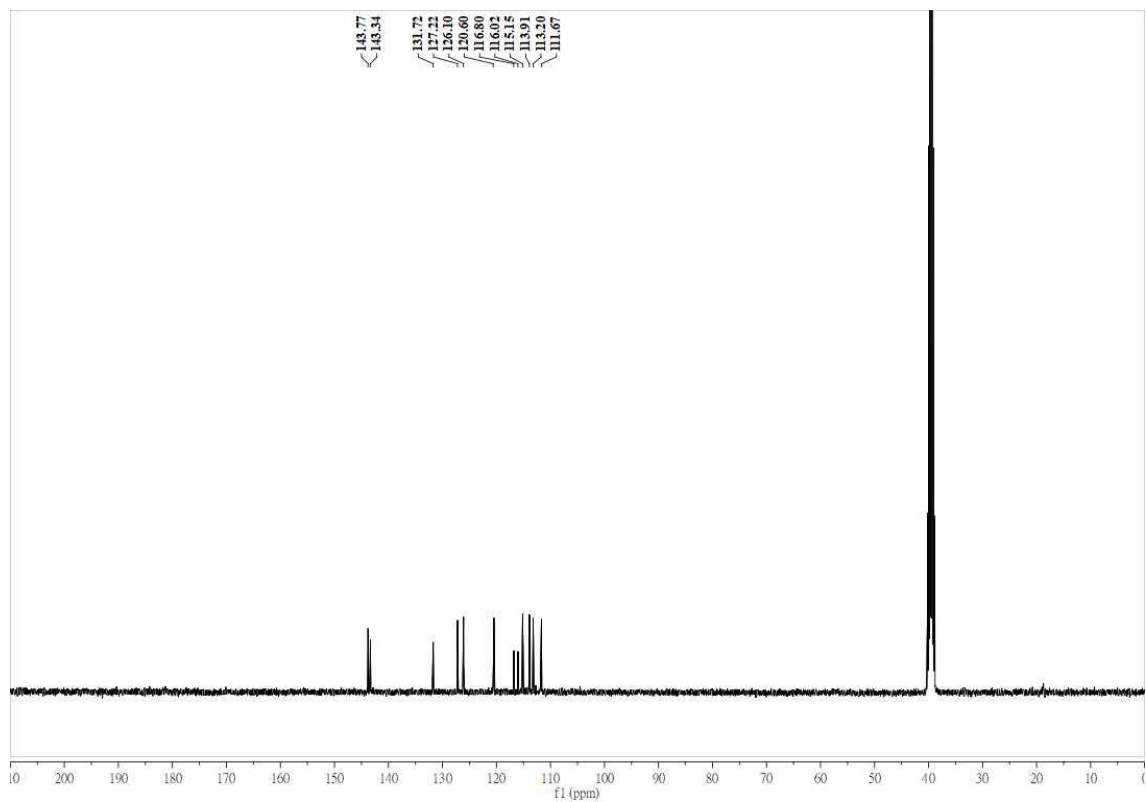
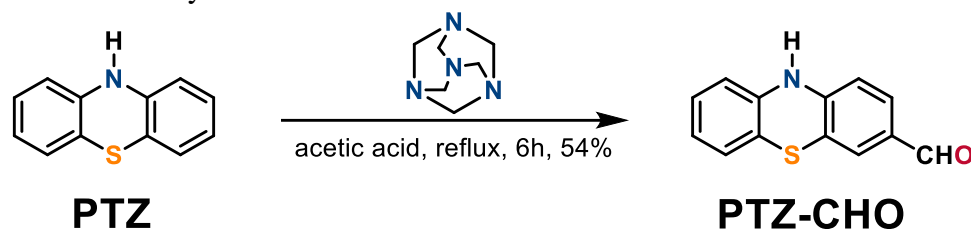


Figure S12. ^{13}C NMR of PTZ-NH₂.

3. Synthesis of **PTZ-CHO**

Scheme S3. Synthetic route of **PTZ-CHO**.



To the solution of phenothiazine (1 g, 5.02 mmole, 1 equiv.) and 1, 3, 5, 7-Tetraazatricyclo [3.3.1.1.3,7]decane (0.774 g, 5.52 mmole, 1.1 equiv.) in the acetic acid (10 ml) was refluxed overnight. After completion of reaction, the reactant was cooled to room temperature and then poured in the saturated sodium bicarbonate in the ice bath. After that, the reactant was extracted with ethyl acetate and brine. The organic layer was separated, dried over MgSO_4 and concentrated by rotavapor. The crude product could be purified by silica column (ethyl acetate: hexane =1: 4 with 1% TEA). The pure product **PTZ-CHO** was light yellow powder (2.71 mmole, 0.615 g, 54.3%). mp=176°C, FT-IR (cm^{-1}): 3339, 2838,2749, 1659, 1556, 1469, 1199, 805. ^1H NMR (400 MHz, DMSO) δ 9.64 (s, 1H), 9.25 (s, 1H), 7.49 (d, J = 8.1 Hz, 1H), 7.36 (s, 1H), 7.00 (t, J = 6.9 Hz, 1H), 6.91 (d, J = 7.4 Hz, 1H), 6.81 (t, J = 7.3 Hz, 1H), 6.71 (dd, J = 16.7, 7.9 Hz, 2H). ^{13}C NMR (101 MHz, DMSO) δ 189.92, 147.12, 139.95, 139.58, 130.53, 127.86, 127.39, 126.26, 123.10, 116.62, 115.81, 115.22, 113.84. HRMS (ESI-TOF) m/z : $[\text{M}+\text{H}]^+$ Calc'd for $\text{C}_{13}\text{H}_9\text{NOS}$ [228.04]; Found 228.04.

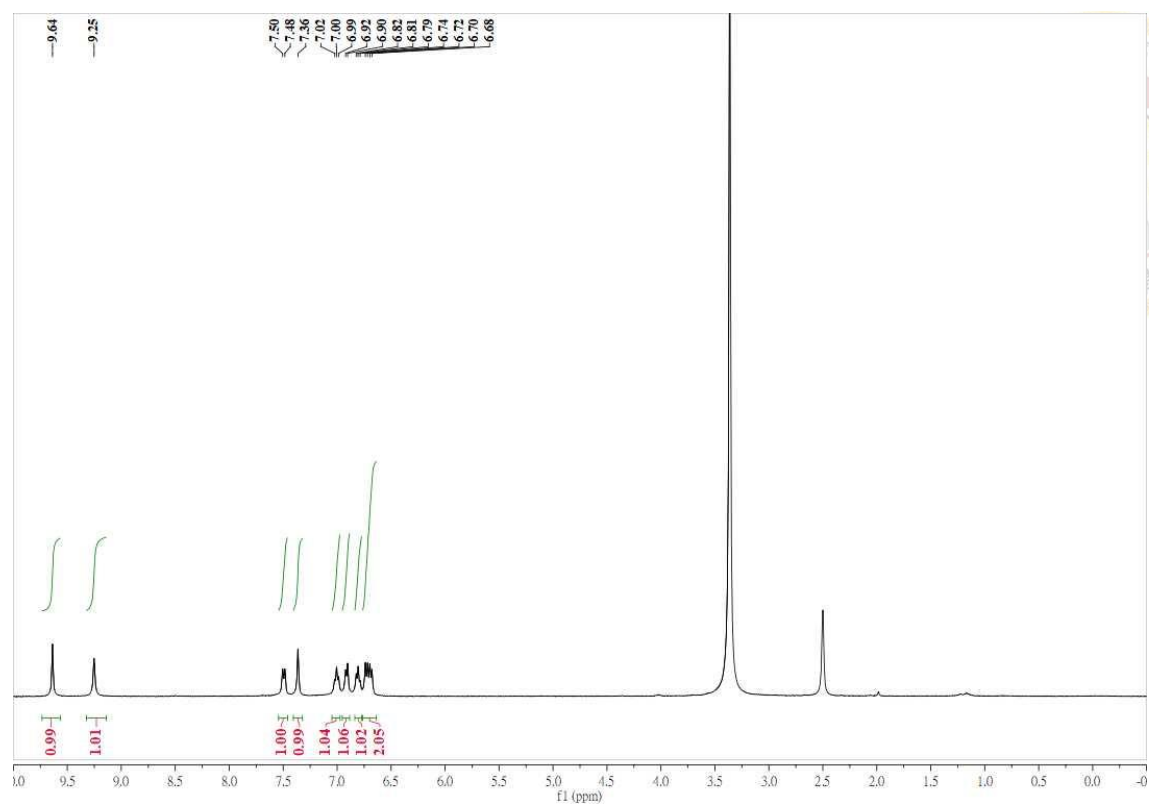


Figure S13. ^1H NMR of PTZ-CHO.

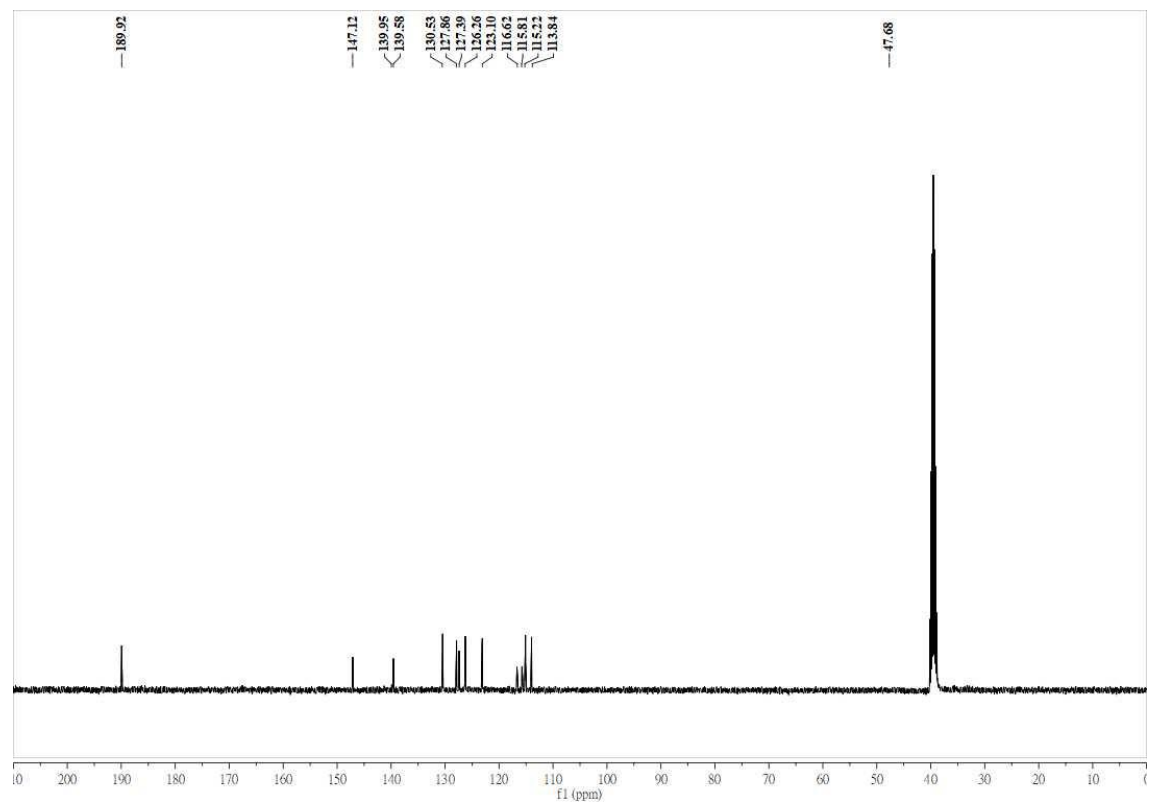
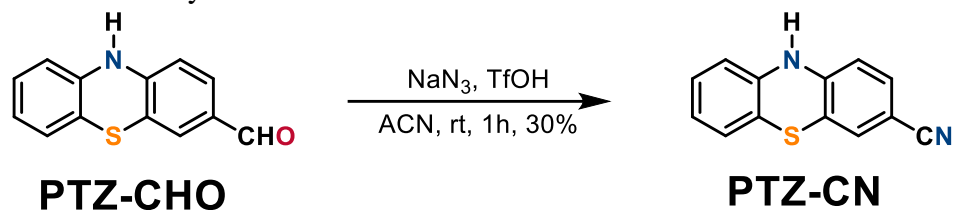


Figure S14. ^{13}C NMR of PTZ-CHO.

4. Synthesis of **PTZ-CN**

Scheme S4. Synthetic route of **PTZ-CN**.



To the solution of PTZ-CHO (0.3 g, 1.32 mmole, 1 equiv.) and sodium azide (0.258 g, 3.96 mmole, 3 equiv.) in the acetonitrile (10 ml) was fast stirred and added by triflic acid (0.70ml, 7.93mmole, 6equiv.) in the room temperature for one hour. After completion of reaction, the reactant was extracted with ethyl acetate and brine. The organic layer was separated, dried over MgSO_4 and then concentrated by rotavapor. The crude product was purified by silica column (ethyl acetate: hexane= 1: 3). The pure product **PTZ-CN** is green powder (0.089g, 0.396mmole, 30%). mp = 161°C, FT-IR (cm^{-1}): 3322, 3162, 3054, 2219, 1557, 1514, 1478, 814. ^1H NMR (400 MHz, DMSO) δ 9.18 (s, 1H), 7.37 (d, J = 15.1 Hz, 2H), 7.01 (t, J = 7.6 Hz, 1H), 6.91 (d, J = 7.6 Hz, 1H), 6.81 (t, J = 7.4 Hz, 1H), 6.75 – 6.64 (m, 2H). ^{13}C NMR (101 MHz, DMSO) δ 145.91, 139.71, 132.14, 129.47, 127.97, 126.36, 123.24, 118.85, 117.23, 115.46, 115.10, 114.19, 102.89. HRMS (ESI-TOF) m/z: $[\text{M}+\text{H}]^+$ Calc'd for $\text{C}_{13}\text{H}_8\text{N}_2\text{S}$ [225.04]; Found 225.04.

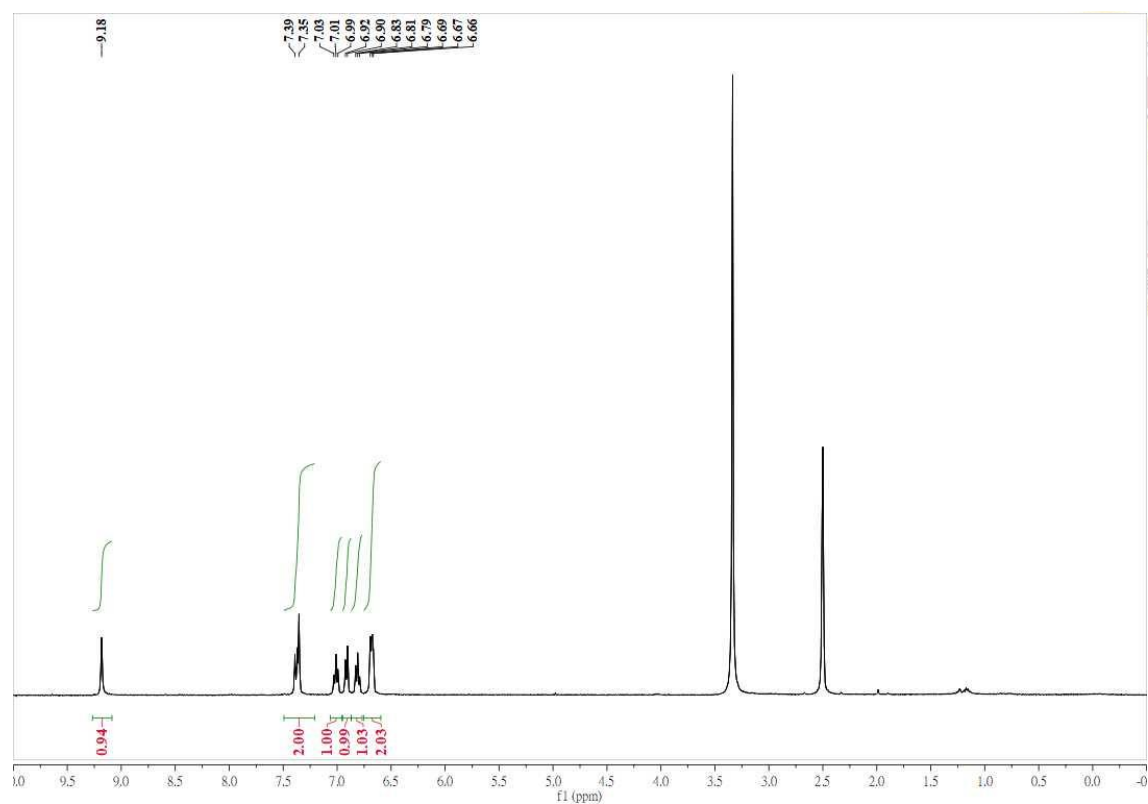


Figure S15. ^1H NMR of PTZ-CN.

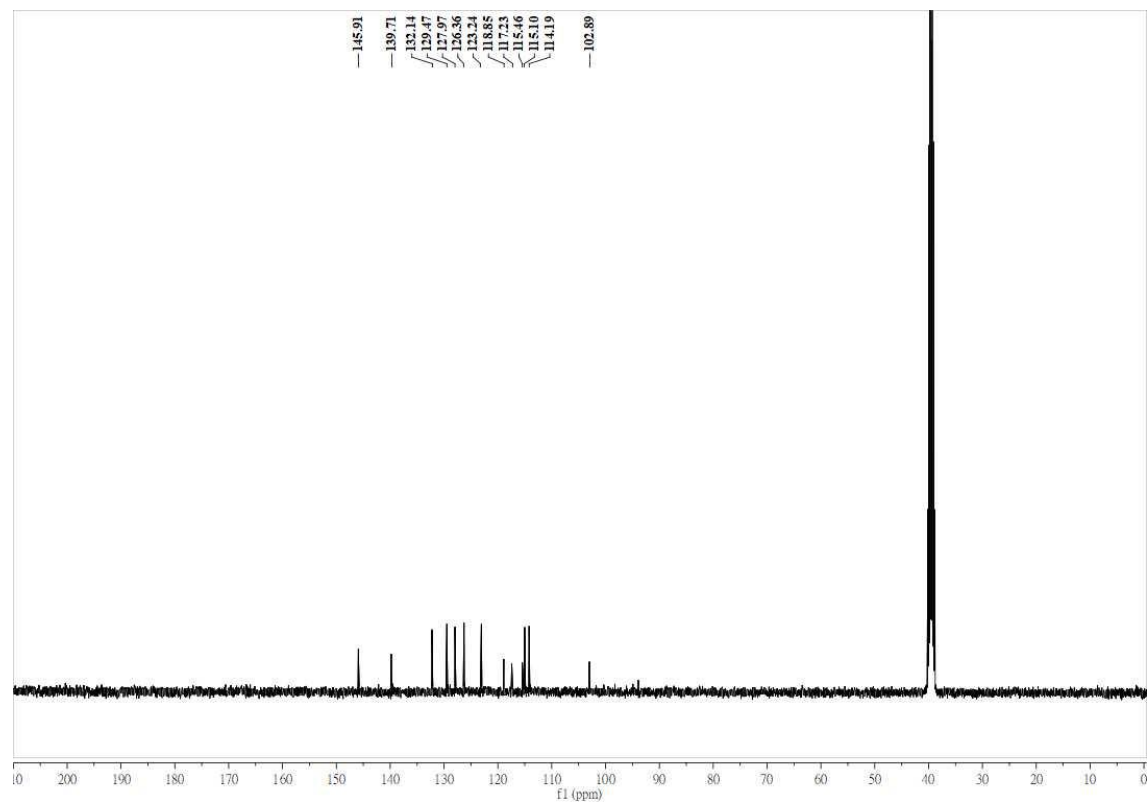
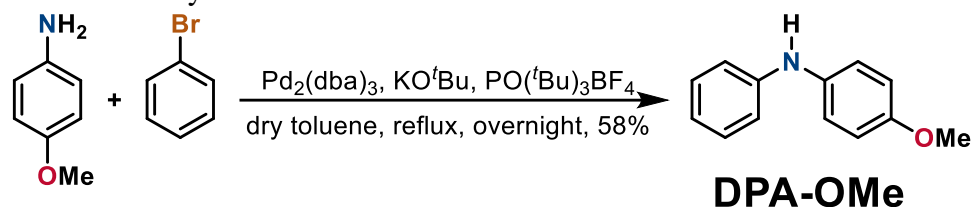


Figure S16. ^{13}C NMR of PTZ-CN.

5. Synthesis of **DPA-OMe**

Scheme S5. Synthetic route of **DPA-OMe**.



To the solution of 4-methoxyaniline (3.53 g, 28.7 mmole, 1.5 equiv.), bromobenzene (3.00g, 19.1mmole, 1.0equiv.), potassium tert-butoxide (2.79 g, 24.8 mmole, 1.3 equiv.), Tri-tert-butylphosphonium tetrafluoroborate (330mg, 1.15 mmole, 0.06 equiv.) and Tris(dibenzylideneacetone)dipalladium(0) (52.4mg, 0.057mmole, 0.03equiv.) in dry toluene (50ml) was degassed by nitrogen and stirred in the room temperature overnight. After completion of reaction, the reactant was extracted with ethyl acetate and brine. The organic layer was separated, dried over MgSO_4 , and then concentrated by rotavapor. The crude product could be purified by silica column (ethyl acetate: hexane = 1:15). The pure compound **DPA-OMe** was orange powder (2.12g, 11.0mmole, 57.9 %). mp = 96°C, FT-IR (cm^{-1}): 3387, 3008, 2959, 2931, 2837, 1596, 1502, 1317, 1182, 1107, 881, 752. ^1H NMR (400 MHz, DMSO) δ 7.82 (s, 1H), 7.15 (t, $J = 8.7$ Hz, 2H), 7.03 (d, $J = 8.7$ Hz, 2H), 6.95 – 6.80 (m, 4H), 6.70 (t, 1H), 3.71 (s, 3H). ^{13}C NMR (101 MHz, DMSO) δ 153.67, 145.12, 135.99, 129.63, 120.20, 118.38, 114.75, 114.35, 55.01. HRMS (ESI-TOF) m/z: $[\text{M}+\text{H}]^+$ Calc'd for $\text{C}_{13}\text{H}_{13}\text{NO}$ [200.10]; Found 200.10.

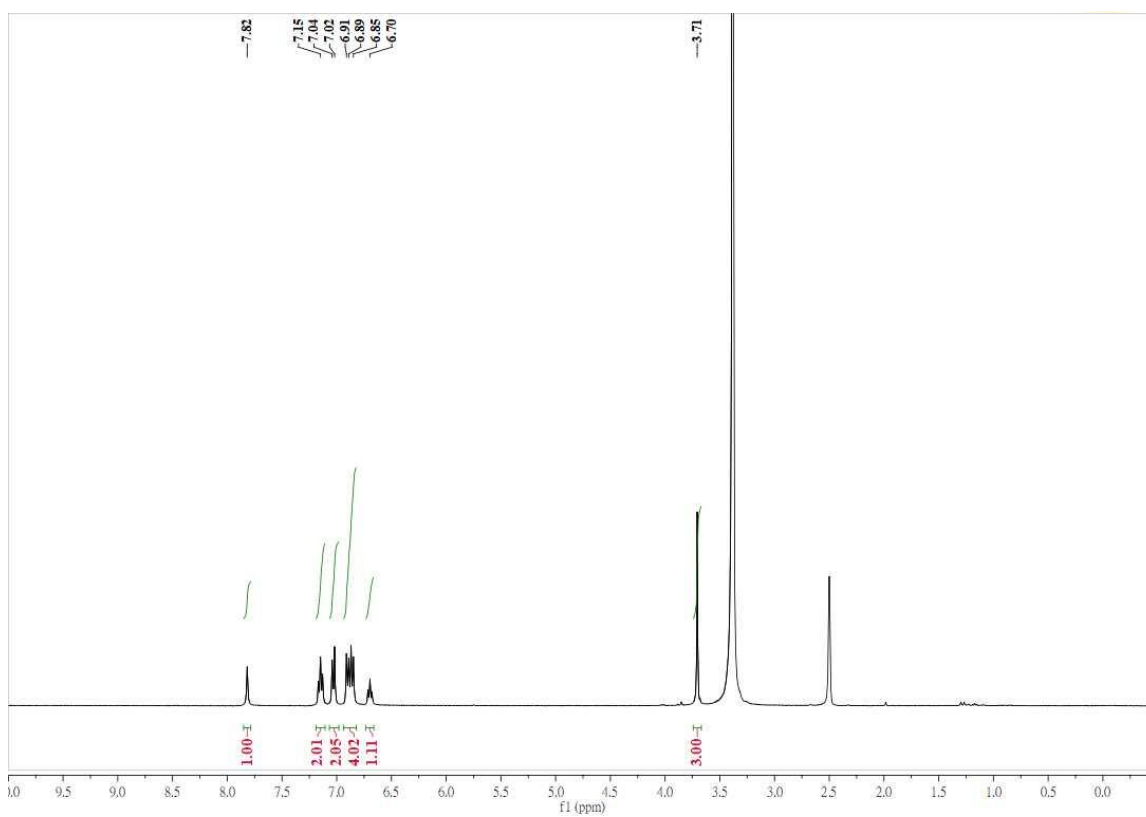


Figure S17. ^1H NMR of DPA-OMe.

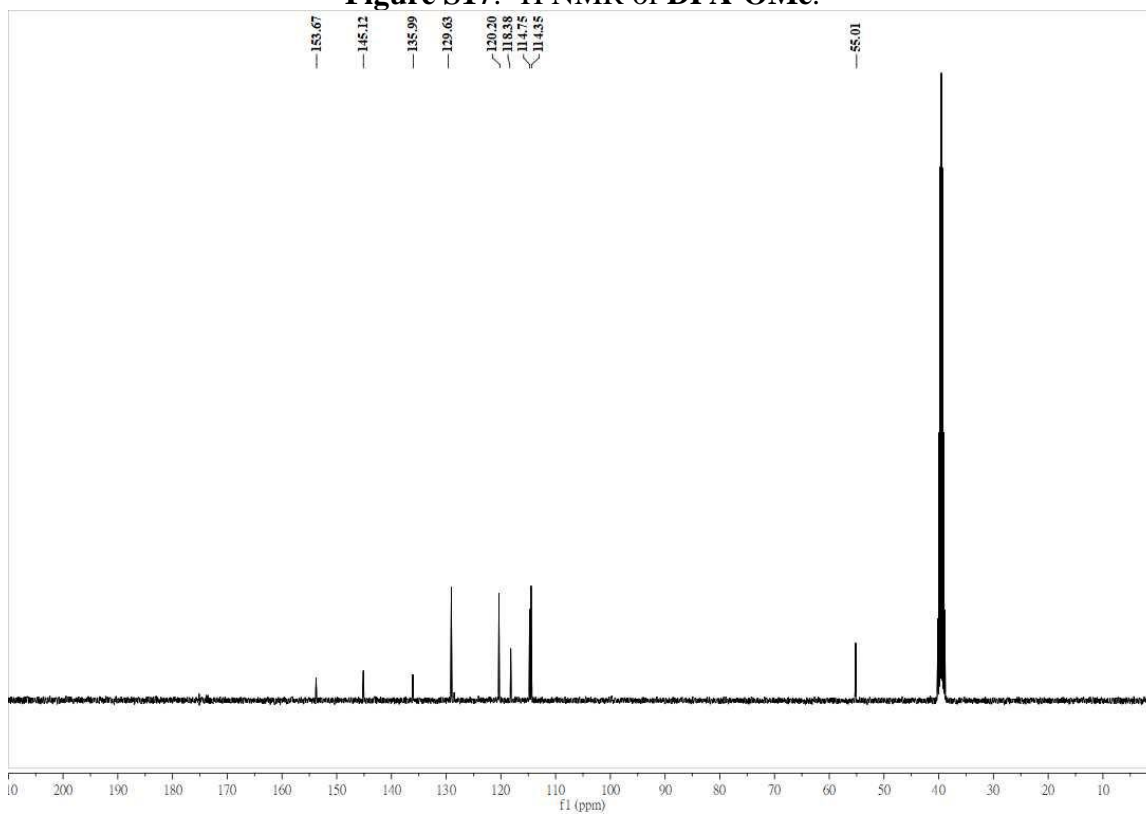
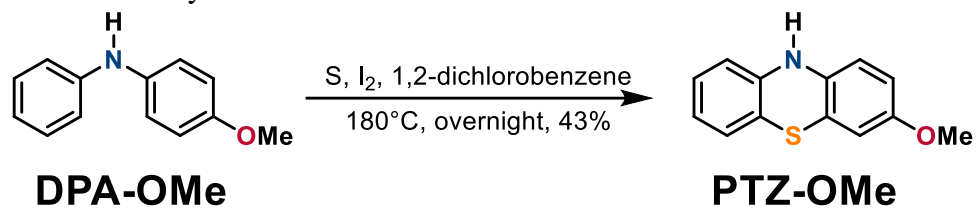


Figure S18. ^{13}C NMR of DPA-OMe.

6. Synthesis of **PTZ-OMe**

Scheme S6. Synthetic route of **PTZ-OMe**.



To the solution of **DPA-OMe** (1g, 5.02 mmole, 1 equiv.), sulfur (320 mg, 10 mmole, 2 equiv.) and iodine (35.7 mg, 0.1406 mmole, 0.028 equiv.) in 1, 2-dichlorobenzene (10 ml) was degassed by nitrogen and refluxed overnight. After completion of reaction, the reactant was extracted by ethyl acetate and brine. The organic layer was separated, dried over MgSO_4 and then concentrated by rotavapor. The crude product could be purified by silica column (ethyl acetate: hexane= 1:8). The pure compound **PTZ-OMe** was grey powder (0.50 g, 2.18 mmole, 43.4%). mp = 146°C , FT-IR (cm^{-1}): 3366, 3064, 2960, 1579, 1461, 1237, 1180, 816, 742. ^1H NMR (400 MHz, DMSO) δ 8.37 (s, 1H), 6.97 (s, 1H), 6.91 (s, 1H), 6.72 (s, 1H), 6.69 – 6.53 (m, 4H), 3.65 (s, 3H). ^{13}C NMR (101 MHz, DMSO) δ 154.58, 142.71, 135.69, 127.51, 125.96, 121.37, 117.42, 115.89, 115.00, 114.34, 113.15, 111.35, 55.59. HRMS (ESI-TOF) m/z: $[\text{M}+\text{H}]^+$ Calc'd for $\text{C}_{13}\text{H}_{11}\text{N}_2\text{O}_2\text{S}$ [230.06]; Found 230.06.

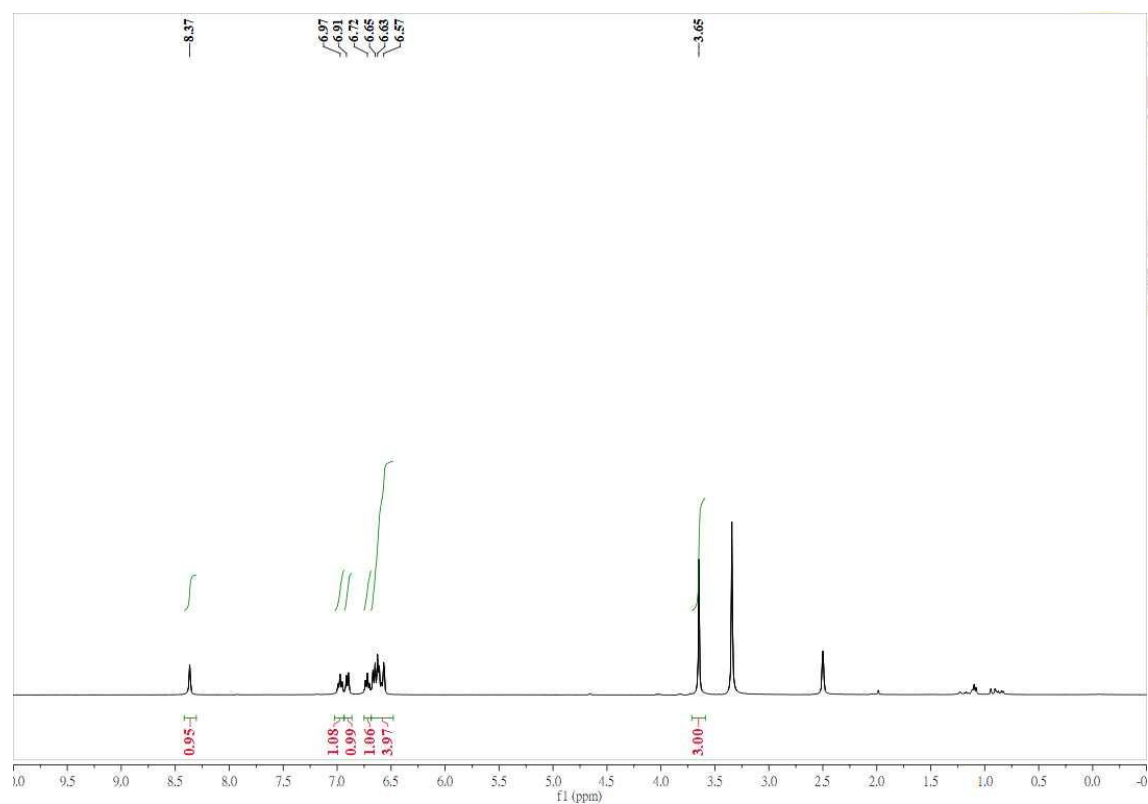


Figure S19. ^1H NMR of PTZ-OMe.

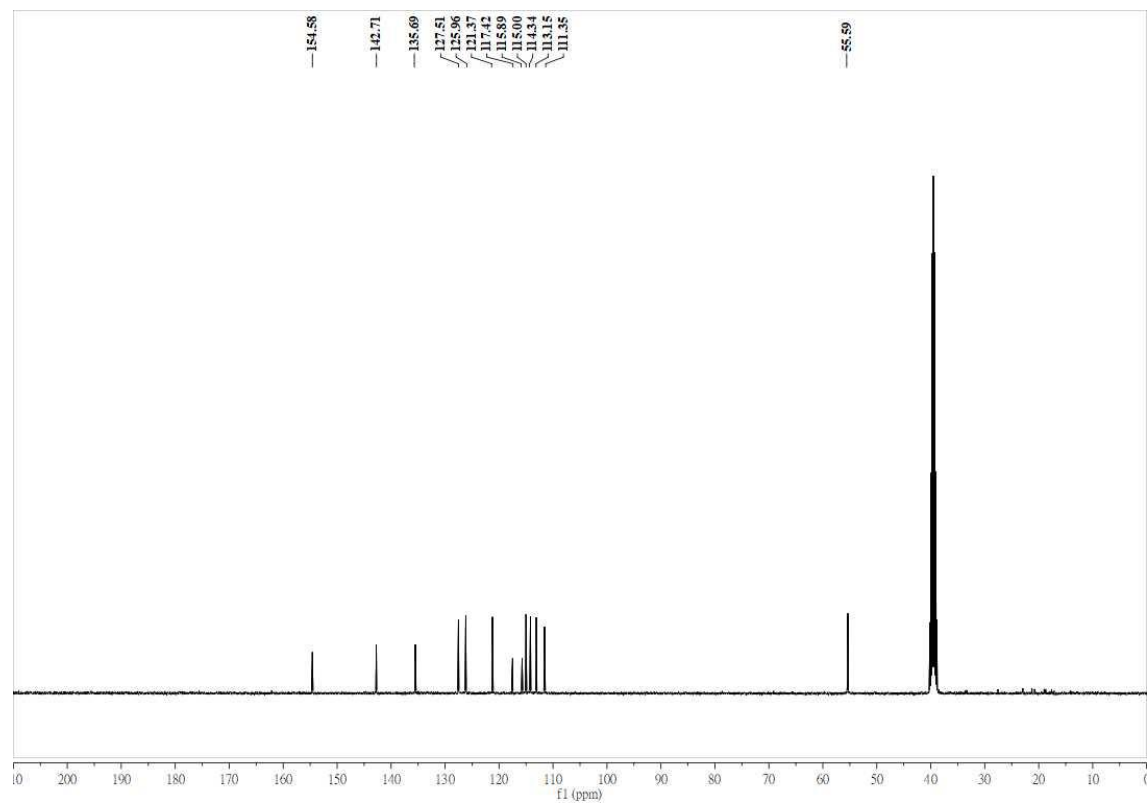


Figure S20. ^{13}C NMR of PTZ-OMe.

D. Cyclic Voltammetry

1. Cyclic Voltammetry graph

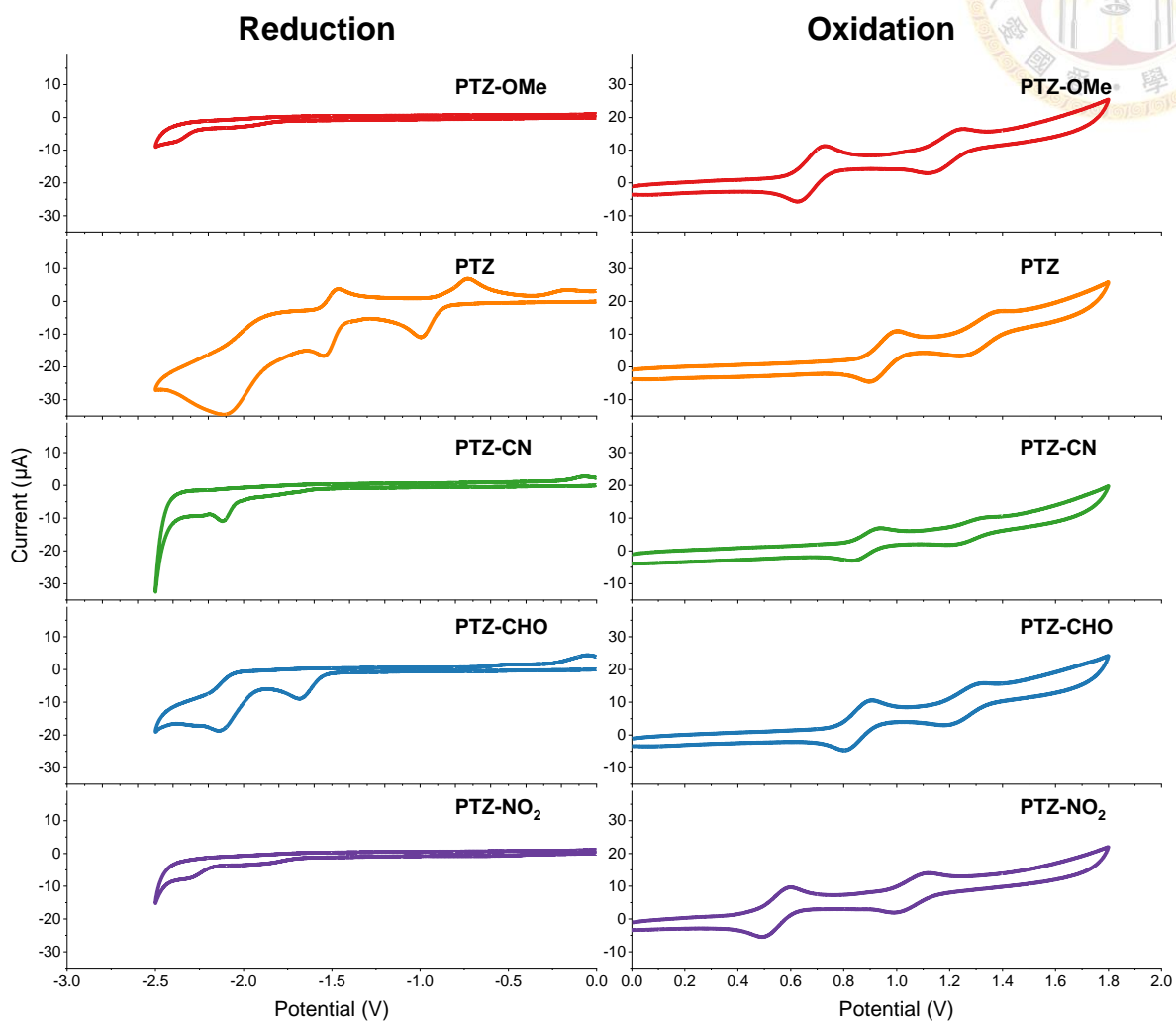
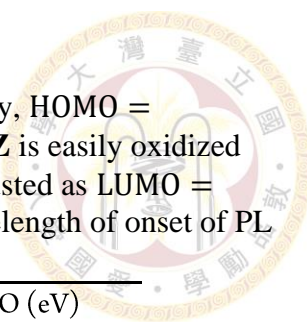


Figure S21. Cyclic voltammograms of five entitled molecules. Reduction curves of **PTZ** derivatives are irreversible since they are easily oxidized.

2. HOMO LUMO energy

Table S3. HOMO LUMO energy calculated from CV and PL data. Usually, HOMO = $-(4.8 + E_{oxi}^D - E_{oxi}^{Fc})$ and LUMO = $-(4.8 + E_{red}^A - E_{red}^{Fc})$. However, **PTZ** is easily oxidized when measuring reduction potential, so the calculation of LUMO was adjusted as LUMO = HOMO + $E_{PL\ onset}$, where $E_{PL\ onset}$ is the energy converted from the wavelength of onset of PL spectra, which is 420 nm is our case.

Molecule	$E_{1/2}^{oxi}$ (V)	$E_{1/2}^{red}$ (V)	HOMO (eV)	LUMO (eV)
PTZ-OMe	0.486, 0.594	-2.118	-4.80	-1.85
PTZ	0.628, 0.728	-2.020	-4.94	-1.99
PTZ-CN	0.828, 0.943	-2.121	-5.14	-2.19
PTZ-CHO	0.800, 0.910	-1.684	-5.12	-2.16
PTZ-NO ₂	0.842, 1.002	-0.997, -0.731	-5.16	-2.20



E. Computational approach

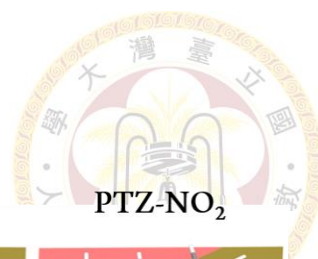
Geometries of the ground state for the titled compounds were optimized by the density functional theory (DFT) method. The electronically excited-state structures with relevant photophysical properties were calculated by time-dependent density functional theory (TD-DFT) method with m062x and b3lyp hybrid function in combination with a polarizable continuum model (PCM) in cyclohexane, and 6-31+G(d,p) basis set for all atoms. The absorbance and emission wavelength from m062x method shown less deviation from experimental data. All theoretical calculations were performed using the Gaussian 09 program. Detail of the supplementary are elaborated below.

Table S4. Calculated wavelength (λ), oscillator strength (f) and orbital transition for five entitled molecules with m062x.

Molecule	Absorption		Fluorescence	
	Energy gap, O.S., and transition		Energy gap, O.S., and transition	
PTZ-OMe	4.11 eV, 301.7 nm. f = 0.0041		3.01 eV, 412.32 nm. f = 0.0061	
	HOMO \rightarrow LUMO	18.81%	LUMO \rightarrow HOMO	95.97%
	HOMO \rightarrow LUMO+1	68.03%		
	HOMO \rightarrow LUMO+2	3.25%		
PTZ	4.09 eV, 302.92 nm. f = 0.0007		2.95 eV, 420.15 nm. f = 0.008	
	HOMO \rightarrow LUMO	91.99%	LUMO \rightarrow HOMO	97.44%
PTZ-CN	3.84 eV, 323.28 nm. f = 0.0741		2.80 eV, 443.01 nm. f = 0.0559	
	HOMO \rightarrow LUMO	84.90%	LUMO \rightarrow HOMO	94.82%
	HOMO \rightarrow LUMO+1	4.41%		
	HOMO \rightarrow LUMO+2	2.00%		
PTZ-CHO	3.64 eV, 340.2 nm. f = 0.1248		2.68 eV, 462.76 nm. f = 0.1067	
	HOMO \rightarrow LUMO	83.44%	LUMO \rightarrow HOMO	92.05%
	HOMO \rightarrow LUMO+2	2.95%	LUMO+3 \rightarrow HOMO	2.52%
	HOMO \rightarrow LUMO+4	3.35%		
	HOMO-4 \rightarrow LUMO	4.13%		
PTZ-NO ₂	3.43 eV, 361.92 nm. f = 0.1873		2.50 eV, 496.11 nm. f = 0.1694	
	HOMO \rightarrow LUMO	89.26%	LUMO \rightarrow HOMO	92.38%
	HOMO \rightarrow LUMO+2	2.99%	LUMO+2 \rightarrow HOMO	2.86%
	HOMO \rightarrow LUMO+4	2.83%		

Table S5. Calculated wavelength (λ), oscillator strength (f) and orbital transition for five entitled molecules with b3lyp.

Molecule	Absorption	Fluorescence
	Energy gap, O.S., and transition	Energy gap, O.S., and transition
PTZ-OMe	3.6428 eV, 340.36 nm. f = 0.0012	2.6956 eV, 459.96 nm. f = 0.0058
	HOMO \rightarrow LUMO 58.03%	HOMO \leftarrow LUMO 98.19%
	HOMO \rightarrow LUMO+1 38.77%	
PTZ	3.6452 eV, 340.13 nm. f = 0.0014	2.7474 eV, 451.28 nm. f = 0.0042
	HOMO \rightarrow LUMO 98.02%	LUMO \rightarrow HOMO 99.22%
PTZ-CN	3.3094 eV, 374.64 nm. f = 0.0879	2.5272 eV, 490.6 nm. f = 0.0636
	HOMO \rightarrow LUMO 94.11%	HOMO \leftarrow LUMO 97.48%
	HOMO \rightarrow LUMO+1 2.20%	
PTZ-CHO	3.001 eV, 413.14 nm. f = 0.1292	2.3138 eV, 535.84 nm. f = 0.1004
	HOMO \rightarrow LUMO 95.96%	HOMO \leftarrow LUMO 97.43%
PTZ-NO ₂	2.5222 eV, 491.58 nm. f = 0.1675	1.8999 eV, 652.57 nm. f = 0.1407
	HOMO \rightarrow LUMO 97.76%	HOMO \leftarrow LUMO 98.36%



1. Ground state and excited state optimized structure

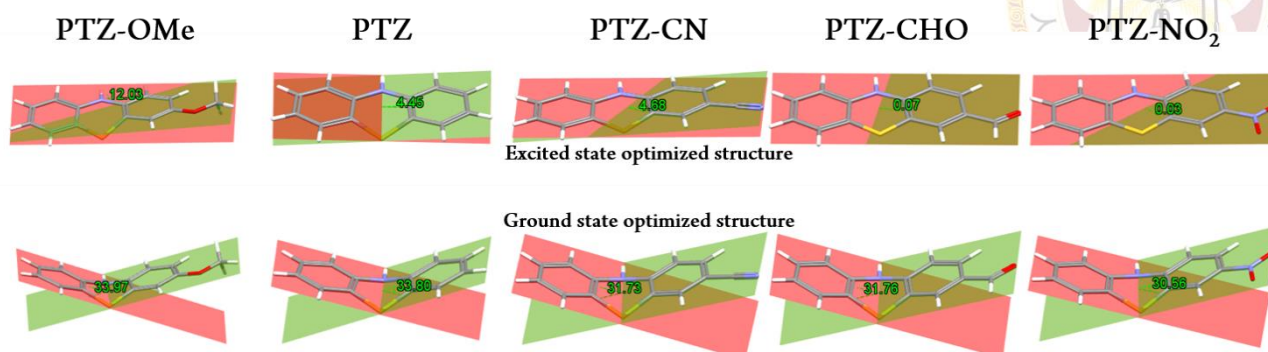


Figure S22. Ground state and excited state optimized structure, with bending angle shown. Red plane was calculated from six carbons in the left benzene ring, green plane was calculated from six carbons in the right benzene ring, and the bending angle was defined as the smaller angle between red and green plane.

2. Ground state optimized orbital

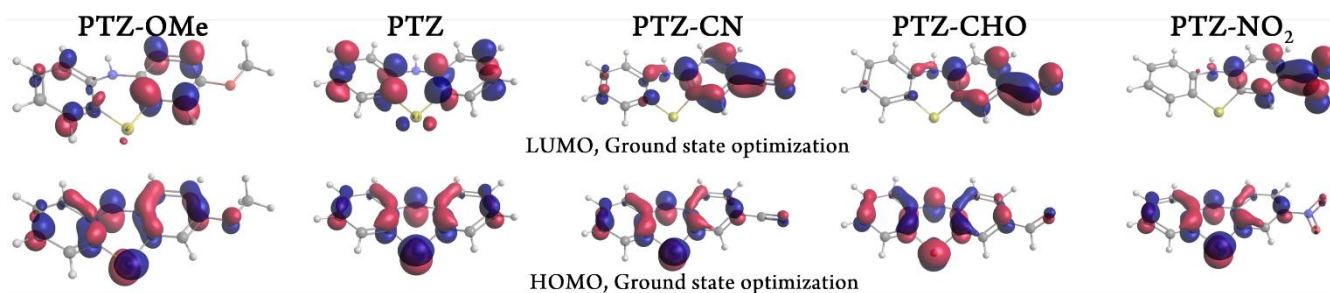


Figure S23. Ground state optimization of LUMO (upper) and HOMO (lower) orbitals for PTZ-OMe, PTZ, PTZ-CN, PTZ-CHO, and PTZ-NO₂ in cyclohexane.

3. Distance definition of r_c , r_{D^+} , and r_{A^-}

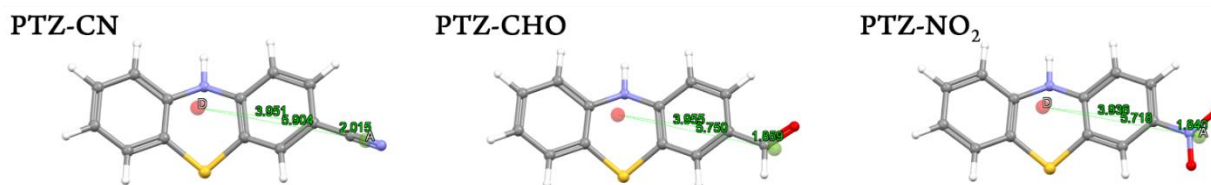


Figure S24. Ground state optimized structures in dichloromethane with the definition of r_c , r_{D^+} , and r_{A^-} . A centroid of 22 atoms without the substituted group was calculated as D, the red sphere; another centroid of the substituted group was calculated as A, the green sphere. r_c is the \overline{DA} distance, r_{D^+} is the $\overline{DC_3}$ distance, and r_{A^-} is the $\overline{C_3A}$ distance.

F. Crystal data and structure refinement

1. Crystallography of PTZ-OMe



Table S6. Crystal data and experimental details for **PTZ-OMe**.

Empirical formula	C13 H10 N O S
Formula weight	228.28
Crystal system	Monoclinic
Space group	P2 ₁ /c
Unit cell dimensions	a = 5.7812(7) Å b = 7.7504(14) Å c = 23.437(5) Å
Volume	1050.0(3) Å ³
Z	4
F(000)	476
Density (calculated)	1.444 Mg/m ³
Wavelength	0.71073 Å
Cell parameters reflections used	321
Theta range for Cell parameters	3.5250 to 24.3760°.
Absorption coefficient	0.282 mm ⁻¹
Temperature	100(2) K
Crystal size	0.20 x 0.10 x 0.01 mm ³
Diffractometer	Xcalibur, Atlas, Gemini
Absorption correction	Semi-empirical from equivalents
Max. and min. transmission	1.00000 and 0.91230
No. of measured reflections	2846
No. of independent reflections	2846 [R(int) = 0.1800]
No. of observed [I>2 σ (I)]	1390
Completeness to theta = 25.242°	99.8 %
Theta range for data collection	3.151 to 27.495°.
Final R indices [I>2 σ (I)]	R1 = 0.0711, wR2 = 0.0927
R indices (all data)	R1 = 0.1615, wR2 = 0.1090
Goodness-of-fit on F ²	0.841
No. of reflections	2846
No. of parameters	146
No. of restraints	0
Largest diff. peak and hole	0.479 and -0.448 e.Å ⁻³

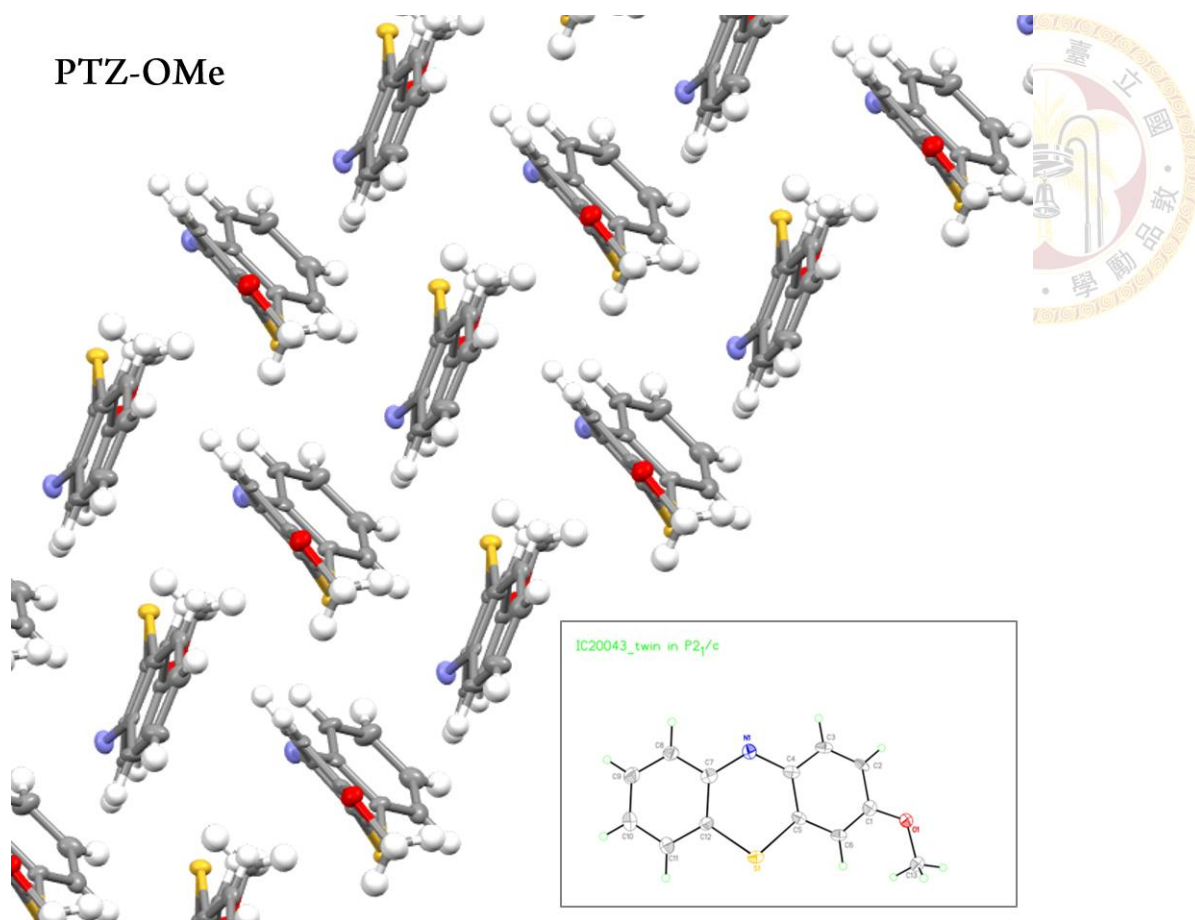


Figure S25. X-ray crystal structure of PTZ-OMe.

2. Crystallography of PTZ

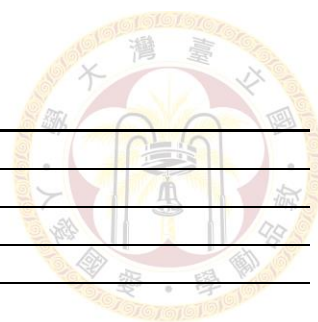
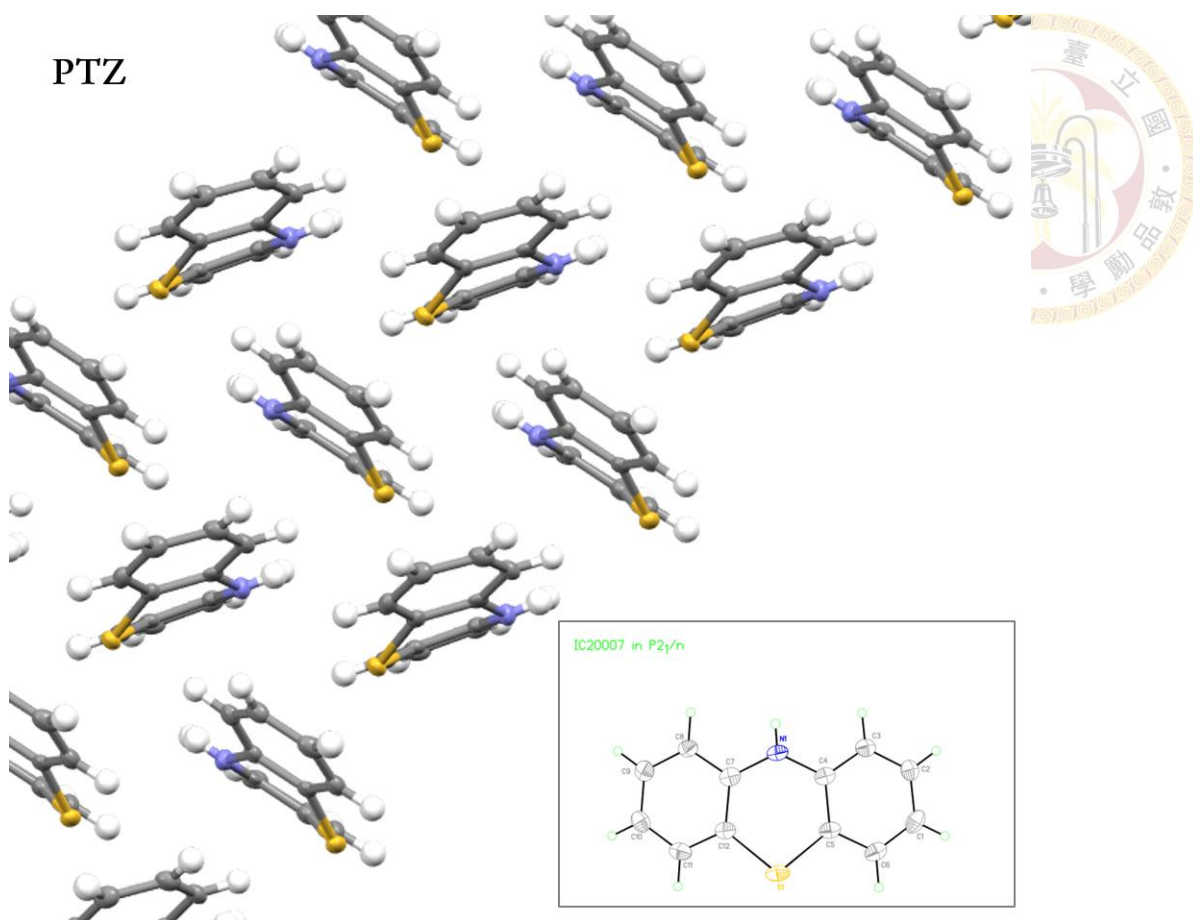


Table S7. Crystal data and experimental details for **PTZ**.

Empirical formula	C ₁₂ H ₉ N S
Formula weight	199.26
Crystal system	Monoclinic
Space group	P2 ₁ /n
Unit cell dimensions	a = 5.8205(3) Å b = 7.7778(4) Å c = 20.7569(17) Å
Volume	936.12(10) Å ³
Z	4
F(000)	416
Density (calculated)	1.414 Mg/m ³
Wavelength	0.71073 Å
Cell parameters reflections used	1506
Theta range for Cell parameters	3.5560 to 27.3880°.
Absorption coefficient	0.297 mm ⁻¹
Temperature	100(2) K
Crystal size	0.20 x 0.15 x 0.10 mm ³
Diffractometer	Xcalibur, Atlas, Gemini
Absorption correction	Semi-empirical from equivalents
Max. and min. transmission	1.00000 and 0.67271
No. of measured reflections	4841
No. of independent reflections	2080 [R(int) = 0.0461]
No. of observed [I>2 σ (I)]	1483
Completeness to theta = 25.242°	99.9 %
Theta range for data collection	3.278 to 27.500°.
Final R indices [I>2 σ (I)]	R1 = 0.0681, wR2 = 0.2017
R indices (all data)	R1 = 0.1029, wR2 = 0.2225
Goodness-of-fit on F ²	1.298
No. of reflections	2080
No. of parameters	130
No. of restraints	0
Largest diff. peak and hole	0.623 and -0.432 e.Å ⁻³



3. Crystallography of PTZ-CHO

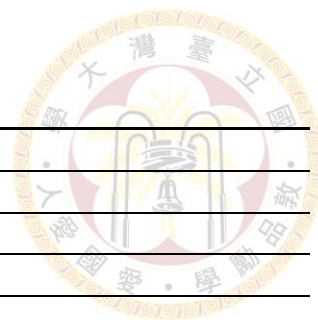


Table S8. Crystal data and experimental details for **PTZ-CHO**.

Empirical formula	C ₁₃ H ₉ N O S
Formula weight	227.27
Crystal system	Orthorhombic
Space group	Pna2 ₁
Unit cell dimensions	a = 7.5021(3) Å b = 23.0537(8) Å c = 5.9064(2) Å
Volume	1021.52(6) Å ³
Z	4
F(000)	472
Density (calculated)	1.478 Mg/m ³
Wavelength	0.71073 Å
Cell parameters reflections used	2469
Theta range for Cell parameters	3.5380 to 29.1410°.
Absorption coefficient	0.289 mm ⁻¹
Temperature	100(2) K
Crystal size	0.20 x 0.20 x 0.15 mm ³
Diffractometer	Xcalibur, Atlas, Gemini
Absorption correction	Semi-empirical from equivalents
Max. and min. transmission	1.00000 and 0.52884
No. of measured reflections	4427
No. of independent reflections	1544 [R(int) = 0.0283]
No. of observed [I>2 σ (I)]	1431
Completeness to theta = 25.242°	99.9 %
Theta range for data collection	2.855 to 27.497°.
Final R indices [I>2 σ (I)]	R1 = 0.0323, wR2 = 0.0969
R indices (all data)	R1 = 0.0366, wR2 = 0.1068
Goodness-of-fit on F ²	0.871
No. of reflections	1544
No. of parameters	148
No. of restraints	1
Absolute structure parameter	0.00(8)
Largest diff. peak and hole	0.304 and -0.247 e.Å ⁻³

PTZ-CHO

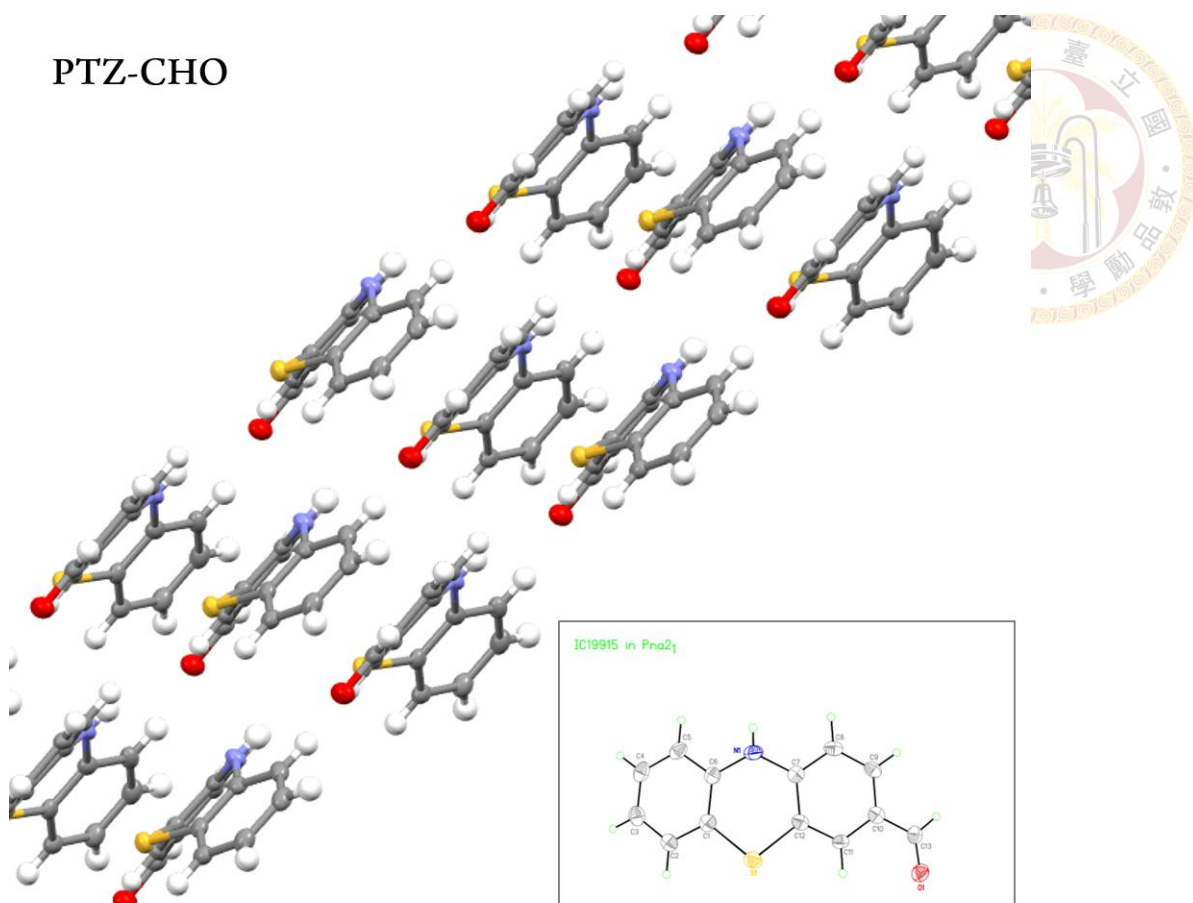


Figure S27. X-ray crystal structure of **PTZ-CHO**.

4. Crystallography of PTZ-NO₂

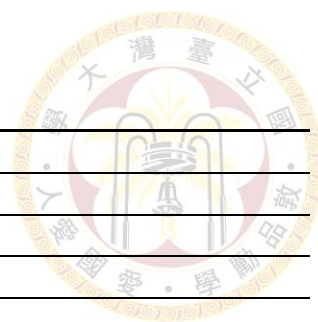


Table S9. Crystal data and experimental details for PTZ-NO₂.

Empirical formula	C ₁₂ H ₈ N ₂ O ₂ S
Formula weight	244.26
Crystal system	Orthorhombic
Space group	Pna2 ₁
Unit cell dimensions	a = 18.0720(19) Å b = 14.985(2) Å c = 3.7505(5) Å
Volume	1015.7(2) Å ³
Z	4
F(000)	504
Density (calculated)	1.597 Mg/m ³
Wavelength	0.71073 Å
Cell parameters reflections used	1125
Theta range for Cell parameters	3.5270 to 28.2310°.
Absorption coefficient	0.307 mm ⁻¹
Temperature	100(2) K
Crystal size	0.20 x 0.10 x 0.10 mm ³
Diffractometer	Xcalibur, Atlas, Gemini
Absorption correction	Semi-empirical from equivalents
Max. and min. transmission	1.00000 and 0.87526
No. of measured reflections	3788
No. of independent reflections	3788 [R(int) = 0.0906]
No. of observed [I>2 σ (I)]	2681
Completeness to theta = 25.242°	99.5 %
Theta range for data collection	3.532 to 27.442°.
Final R indices [I>2 σ (I)]	R1 = 0.0680, wR2 = 0.1587
R indices (all data)	R1 = 0.1007, wR2 = 0.1744
Goodness-of-fit on F ²	1.021
No. of reflections	3788
No. of parameters	158
No. of restraints	1
Absolute structure parameter	0.38(14)
Largest diff. peak and hole	0.866 and -0.925 e.Å ⁻³

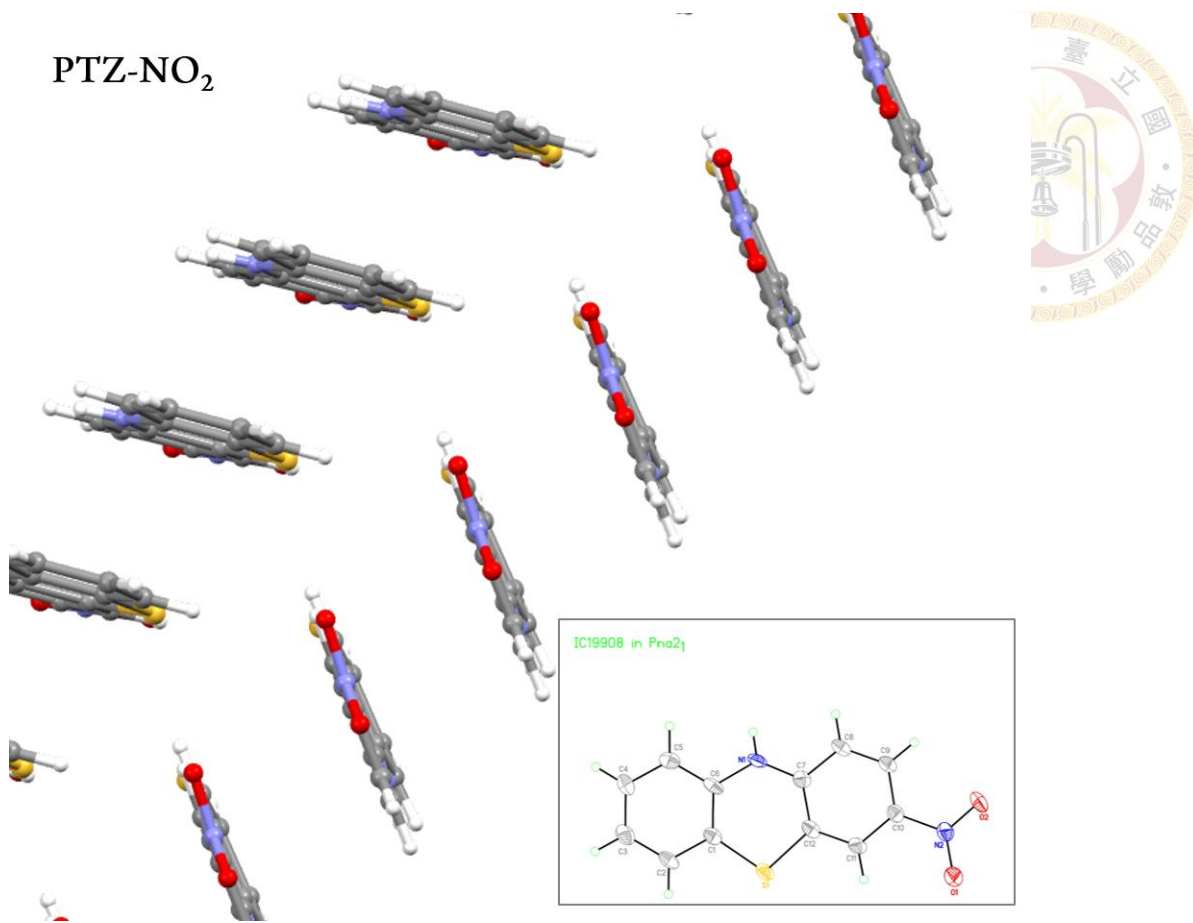
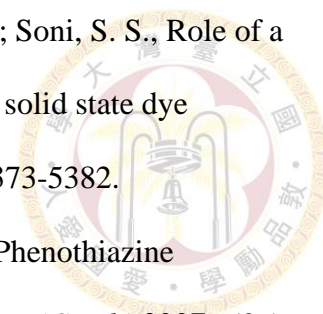


Figure S28. X-ray crystal structure of **PTZ-NO₂**.

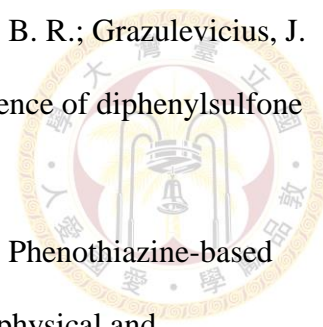
X. Reference

1. Ohlow, M. J.; Moosmann, B., Phenothiazine: the seven lives of pharmacology's first lead structure. *Drug Discov Today* **2011**, *16* (3-4), 119-31.
2. Mitchell, S. C., Phenothiazine: the parent molecule. *Curr Drug Targets* **2006**, *7* (9), 1181-9.
3. Galgoczy, L.; Bacsi, A.; Homa, M.; Viragh, M.; Papp, T.; Vagvolgyi, C., In vitro antifungal activity of phenothiazines and their combination with amphotericin B against different *Candida* species. *Mycoses* **2011**, *54* (6), e737-43.
4. Kristiansen, J. E.; Vergmann, B., The antibacterial effect of selected phenothiazines and thioxanthenes on slow-growing mycobacteria. *Acta Pathol Microbiol Immunol Scand B* **1986**, *94* (6), 393-8.
5. Harwood, P. D., Parasitological Reviews - the Anthelmintic Properties of Phenothiazine. *Exp Parasitol* **1953**, *2* (4), 428-455.
6. Burn, J. H., The pharmacology of chlorpromazine and promethazine. *Proc R Soc Med* **1954**, *47* (8), 617-21.
7. Swazey, J. P., *Chlorpromazine in psychiatry: A study of therapeutic innovation*. MIT Press Cambridge, MA: 1974.
8. Cosofret, V. V.; Buck, R. P., Phenothiazine drug poly(vinyl chloride) matrix membrane electrodes and their use in pharmaceutical analysis. *Analyst* **1984**, *109* (10), 1321-5.
9. Wu, C.-H.; Bai, L.-Y.; Tsai, M.-H.; Chu, P.-C.; Chiu, C.-F.; Chen, M. Y.; Chiu, S.-J.; Chiang, J.-H.; Weng, J.-R., Pharmacological exploitation of the phenothiazine antipsychotics to develop novel antitumor agents—A drug repurposing strategy. *Scientific Reports* **2016**, *6* (1).
10. Huang, Z.-S.; Meier, H.; Cao, D., Phenothiazine-based dyes for efficient dye-sensitized solar cells. *Journal of Materials Chemistry C* **2016**, *4* (13), 2404-2426.

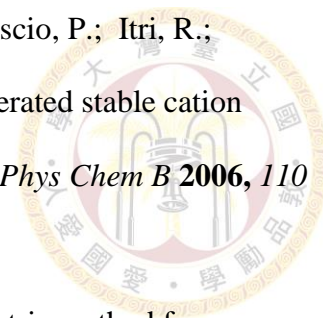




11. Vaghasiya, J. V.; Sonigara, K. K.; Prasad, J.; Beuvier, T.; Gibaud, A.; Soni, S. S., Role of a phenothiazine/phenoxazine donor in solid ionic conductors for efficient solid state dye sensitized solar cells. *Journal of Materials Chemistry A* **2017**, 5 (11), 5373-5382.
12. Tian, H.; Yang, X.; Chen, R.; Pan, Y.; Li, L.; Hagfeldt, A.; Sun, L., Phenothiazine derivatives for efficient organic dye-sensitized solar cells. *Chem Commun (Camb)* **2007**, (36), 3741-3.
13. Blanco, G. D.; Hiltunen, A. J.; Lim, G. N.; Kc, C. B.; Kaunisto, K. M.; Vuorinen, T. K.; Nesterov, V. N.; Lemmetyinen, H. J.; D'Souza, F., Syntheses, Charge Separation, and Inverted Bulk Heterojunction Solar Cell Application of Phenothiazine-Fullerene Dyads. *ACS Appl Mater Interfaces* **2016**, 8 (13), 8481-90.
14. Tanaka, H.; Shizu, K.; Nakanotani, H.; Adachi, C., Dual Intramolecular Charge-Transfer Fluorescence Derived from a Phenothiazine-Triphenyltriazine Derivative. *The Journal of Physical Chemistry C* **2014**, 118 (29), 15985-15994.
15. Okazaki, M.; Takeda, Y.; Data, P.; Pander, P.; Higginbotham, H.; Monkman, A. P.; Minakata, S., Thermally activated delayed fluorescent phenothiazine-dibenzo[a,j]phenazine-phenothiazine triads exhibiting tricolor-changing mechanochromic luminescence. *Chem Sci* **2017**, 8 (4), 2677-2686.
16. Chen, D.-G.; Lin, T.-C.; Chen, Y.-A.; Chen, Y.-H.; Lin, T.-C.; Chen, Y.-T.; Chou, P.-T., Revisiting Dual Intramolecular Charge-Transfer Fluorescence of Phenothiazine-triphenyltriazine Derivatives. *The Journal of Physical Chemistry C* **2018**, 122 (23), 12215-12221.
17. Marghad, I.; Bencheikh, F.; Wang, C.; Manolikakes, S.; Rérat, A.; Gosmini, C.; Kim, D. h.; Ribierre, J.-C.; Adachi, C., Control of the dual emission from a thermally activated delayed fluorescence emitter containing phenothiazine units in organic light-emitting diodes. *RSC Advances* **2019**, 9 (8), 4336-4343.



18. Bezikonnyi, O.; Gudeika, D.; Volyniuk, D.; Mimaite, V.; Sebastine, B. R.; Grazulevicius, J. V., Effect of donor substituents on thermally activated delayed fluorescence of diphenylsulfone derivatives. *Journal of Luminescence* **2019**, *206*, 250-259.
19. Bodedla, G. B.; Justin Thomas, K. R.; Kumar, S.; Jou, J.-H.; Li, C.-J., Phenothiazine-based bipolar green-emitters containing benzimidazole units: synthesis, photophysical and electroluminescence properties. *RSC Advances* **2015**, *5* (106), 87416-87428.
20. Salunke, J. K.; Wong, F. L.; Feron, K.; Manzhos, S.; Lo, M. F.; Shinde, D.; Patil, A.; Lee, C. S.; Roy, V. A. L.; Sonar, P.; Wadgaonkar, P. P., Phenothiazine and carbazole substituted pyrene based electroluminescent organic semiconductors for OLED devices. *Journal of Materials Chemistry C* **2016**, *4* (5), 1009-1018.
21. Zeng, X.-C.; Wang, J.-Y.; Xu, L.-J.; Wen, H.-M.; Chen, Z.-N., Solution-processed OLEDs based on phosphorescent PtAu₂ complexes with phenothiazine-functionalized acetylides. *Journal of Materials Chemistry C* **2016**, *4* (25), 6096-6103.
22. Bejan, A.; Shova, S.; Damaceanu, M.-D.; Simionescu, B. C.; Marin, L., Structure-Directed Functional Properties of Phenothiazine Brominated Dyes: Morphology and Photophysical and Electrochemical Properties. *Crystal Growth & Design* **2016**, *16* (7), 3716-3730.
23. Satoh, Y.; Catti, L.; Akita, M.; Yoshizawa, M., A Redox-Active Heterocyclic Capsule: Radical Generation, Oxygenation, and Guest Uptake/Release. *J Am Chem Soc* **2019**, *141* (31), 12268-12273.
24. Zhou, Z.; Hauke, C. E.; Song, B.; Li, X.; Stang, P. J.; Cook, T. R., Understanding the Effects of Coordination and Self-Assembly on an Emissive Phenothiazine. *J Am Chem Soc* **2019**, *141* (8), 3717-3722.
25. Im, Y.; Kim, M.; Cho, Y. J.; Seo, J.-A.; Yook, K. S.; Lee, J. Y., Molecular Design Strategy of Organic Thermally Activated Delayed Fluorescence Emitters. *Chemistry of Materials* **2017**, *29* (5), 1946-1963.



26. Rodrigues, T.; dos Santos, C. G.; Riposati, A.; Barbosa, L. R.; Di Mascio, P.; Itri, R.; Baptista, M. S.; Nascimento, O. R.; Nantes, I. L., Photochemically generated stable cation radical of phenothiazine aggregates in mildly acid buffered solutions. *J Phys Chem B* **2006**, *110* (25), 12257-65.
27. Upadhyay, K.; Asthana, A.; Tamrakar, R. K., Sensitive spectrophotometric method for determination of some phenothiazine drugs. *Research on Chemical Intermediates* **2014**, *41* (10), 7481-7495.
28. Saucin, M.; Vandevorst, A., Photodynamic Potentialities of Some Phenothiazine-Derivatives. *Radiat Environ Bioph* **1980**, *17* (2), 159-168.
29. Hosseinnezhad, M.; Gharanjig, K.; Moradian, S.; Tafaghodi, S., Synthesis and application of some novel fluorescent heterocyclic disperse dyestuffs based on phenothiazine on polyester. *Arabian Journal of Chemistry* **2015**.
30. Huber, J. R.; Mantulin, W. W., Emission Properties of Aromatic-Amines in Solution - Phenoxazine System. *Journal of the American Chemical Society* **1972**, *94* (11), 3755-3760.
31. Nobuyasu, R. S.; Ren, Z.; Griffiths, G. C.; Batsanov, A. S.; Data, P.; Yan, S.; Monkman, A. P.; Bryce, M. R.; Dias, F. B., Rational Design of TADF Polymers Using a Donor-Acceptor Monomer with Enhanced TADF Efficiency Induced by the Energy Alignment of Charge Transfer and Local Triplet Excited States. *Advanced Optical Materials* **2016**, *4* (4), 597-607.
32. Massie, S. P., The Chemistry of Phenothiazine. *Chem Rev* **1954**, *54* (5), 797-883.
33. Gaina, L.; Cristea, C.; Moldovan, C.; Porumb, D.; Surducan, E.; Deleanu, C.; Mahamoud, A.; Barbe, J.; Silberg, I. A., Microwave-assisted synthesis of phenothiazine and quinoline derivatives. *Int J Mol Sci* **2007**, *8* (2), 70-80.
34. Motiwala, H. F.; Yin, Q.; Aube, J., Improved Schmidt Conversion of Aldehydes to Nitriles Using Azidotrimethylsilane in 1,1,1,3,3,3-Hexafluoro-2-propanol. *Molecules* **2015**, *21* (1), E45.

35. Ernst, J. B.; Schwermann, C.; Yokota, G. I.; Tada, M.; Muratsugu, S.; Doltsinis, N. L.; Glorius, F., Molecular Adsorbates Switch on Heterogeneous Catalysis: Induction of Reactivity by N-Heterocyclic Carbenes. *J Am Chem Soc* **2017**, *139* (27), 9144-9147.
36. Jensen, L. H., Molecular Packing in Organic Crystals. *J Polym Sci Polym Chem Ed* **1970**, (29), 47-54.
37. Kawanishi, Y.; Kitamura, N.; Tazuke, S., Coulombic Effect on Photoinduced Electron-Transfer Reactions between Phenothiazines and Viologens. *J Phys Chem-Us* **1986**, *90* (11), 2469-2475.
38. Yang, S.; Liu, J.; Zhou, P.; He, G., Solvent effects on 3-keto-1H-pyrido[3,2,1-kl]phenothiazine fluorescence in polar and protic solvents. *J Phys Chem B* **2011**, *115* (36), 10692-8.
39. Caspar, J. V.; Meyer, T. J., Application of the Energy-Gap Law to Nonradiative, Excited-State Decay. *J Phys Chem-Us* **1983**, *87* (6), 952-957.
40. Cummings, S. D.; Eisenberg, R., Tuning the excited-state properties of platinum(II) diimine dithiolate complexes. *Journal of the American Chemical Society* **1996**, *118* (8), 1949-1960.
41. Chen, W.; Chen, C. L.; Zhang, Z.; Chen, Y. A.; Chao, W. C.; Su, J.; Tian, H.; Chou, P. T., Snapshotting the Excited-State Planarization of Chemically Locked N,N'-Disubstituted Dihydrodibenzo[a,c]phenazines. *J Am Chem Soc* **2017**, *139* (4), 1636-1644.
42. Baroncini, M.; Bergamini, G.; Ceroni, P., Rigidification or interaction-induced phosphorescence of organic molecules. *Chem Commun (Camb)* **2017**, (13), 2081-2093.
43. Chen, D.-G.; Ranganathan, R.; Lin, J.-A.; Huang, C.-Y.; Ho, M.-L.; Chi, Y.; Chou, P.-T., Ratiometric Tuning of Luminescence: Interplay between the Locally Excited and Interligand Charge-Transfer States in Pyrazolate-Based Boron Compounds. *The Journal of Physical Chemistry C* **2019**, *123* (7), 4022-4028.